iScience

CellPress
OPEN ACCESS

Article

Aging-Associated Extracellular Vesicles Contain Immune Regulatory microRNAs Alleviating Hyperinflammatory State and Immune Dysfunction in the Elderly

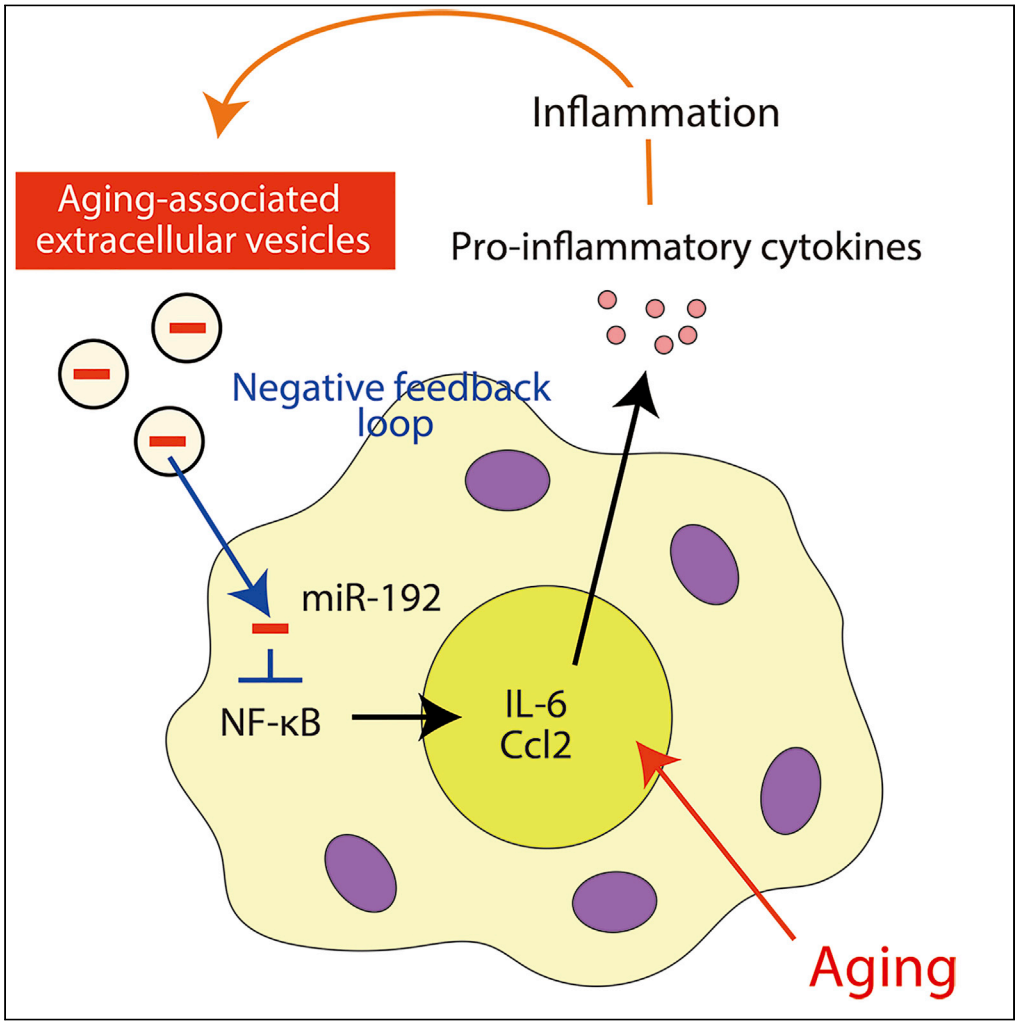

Hirotake Tsukamoto, Takahisa Kouwaki, Hiroyuki Oshiumi

htsukamo@kumamoto-u.ac.jp (H.T.)
oshiumi@kumamoto-u.ac.jp (H.O.)

HIGHLIGHTS

Extracellular vesicle (EV) miR-192 is an aging-associated microRNA

Hyperinflammatory state in aged mice increases miR-192 levels in EVs

miR-192 within EVs attenuates excessive inflammation in aged mice

EVs containing miR-192 improve vaccination efficacy of aged mice

Tsukamoto et al., iScience *23*, 101520
September 25, 2020
https://doi.org/10.1016/j.isci.2020.101520

iScience

CellPress
OPEN ACCESS

Article

Aging-Associated Extracellular Vesicles Contain Immune Regulatory microRNAs Alleviating Hyperinflammatory State and Immune Dysfunction in the Elderly

Hirotake Tsukamoto,[1,*] Takahisa Kouwaki,[1] and Hiroyuki Oshiumi[1,2,*]

SUMMARY

Aging-associated changes in the immune system often lead to immune dysfunction; however, the mechanisms that underlie this phenomenon have yet to be fully elucidated. This study found that the microRNA-192 (miR-192) is an aging-associated immune regulatory microRNA whose concentration was significantly increased in aged extracellular vesicles (EVs) due to the hyperinflammatory state of aged mice. Interestingly, EV miR-192 exhibited anti-inflammatory effects on macrophages. In our aged mouse model, aging was associated with prolonged inflammation in the lung upon stimulation with inactivated influenza whole virus particles (WVP), whereas EV miR-192 alleviated the prolonged inflammation associated with aging. The hyperinflammatory state of aged mice resulted in reduced production of specific antibodies and efficacy of vaccination with WVP; however, EV miR-192 attenuated this hyperinflammatory state and improved vaccination efficacy in aged mice. Our data indicate that aged EVs constitute a negative feedback loop that alleviates aging-associated immune dysfunction.

INTRODUCTION

The innate immune system induces inflammatory responses upon stimulation with pathogen-associated molecular patterns (PAMPs), leading to recruitment and accumulation of myeloid and lymphoid cells that result in the activation of adaptive immune responses (Akira et al., 2006; Banchereau et al., 2000). Toll-like receptors (TLRs) are crucial to the recognition of viral and bacterial infection (Kawai and Akira, 2011). TLR7 senses viral RNA in the endosomes as a PAMP and induces the expression of type I interferon (IFN), pro-inflammatory cytokines, and chemokines, such as interleukin (IL)-6 and CCL2 (Diebold et al., 2004; Hemmi et al., 2002). CL097 and R848 are synthetic ligands for TLR7 that have been used as immune regulatory small molecules (Hemmi et al., 2002). TLR4 recognizes gram-negative bacteria by sensing lipopolysaccharide (LPS) (Medzhitov et al., 1997). The activation of TLRs leads to the maturation of dendritic cells (DCs) and is a key component in the priming of naive T cells (Dalod et al., 2014).

TLR ligands exhibit adjuvant properties during vaccination. For instance, inactivated whole virus particles of the influenza A virus (WVP) are used for vaccination against seasonal influenza and contain viral RNA with adjuvant activity in the form of TLR7 activation (Koyama et al., 2010). Monophosphoryl lipid A, which activates TLR4, is used as an adjuvant in the human papilloma virus vaccine (Garcon et al., 2007). Although vaccination is the first line of prophylaxis against infectious diseases, aging effects on the immune system can lead to immune dysfunctions, resulting in reduced vaccination efficacy in the elderly (Brodin et al., 2015; Ferrucci and Fabbri, 2018; Pinti et al., 2016).

A hyperinflammatory state has been observed in elderly humans and animals, wherein levels of IL-6 and several other pro-inflammatory cytokines in the blood are elevated (Fulop et al., 2014; Pinti et al., 2016). Inflammation itself is a necessary part of immune cell-mediated host protection, with pro-inflammatory cytokines mainly produced by innate immune cells, including macrophages, which are essential components for counteracting viral infections before the development of acquired immunity (Rose-John et al., 2017). However, the onset and termination of inflammatory responses must be tightly regulated because excessive inflammation or unbalanced production of inflammatory cytokines and chemokines can be detrimental to the organism via the amplification of tissue damage and injury and the increased

[1]Department of Immunology, Graduate School of Medical Sciences, Faculty of Life Sciences, Kumamoto University, 1-1-1 Honjo, Kumamoto 860-8556, Japan

[2]Lead Contact

*Correspondence: htsukamo@kumamoto-u.ac.jp (H.T.), oshiumi@kumamoto-u.ac.jp (H.O.)

https://doi.org/10.1016/j.isci.2020.101520

susceptibility to fatal secondary infection in influenza-infected hosts (Peiris et al., 2009; Wang et al., 2014). Interestingly, the hyperinflammatory response has been reported to reduce vaccine efficacy (Fourati et al., 2016; Park et al., 2014). In contrast to pro-inflammatory cytokines, type I IFN production decreases in the elderly alongside an aging-associated decrease in intracellular TRAF3 levels (Molony et al., 2017). The production of free radical and reactive oxygen intermediates by neutrophils and macrophages is also diminished in aged mice (Gomez et al., 2005). Aging-associated changes in the immune system are readily observed, and an accumulating body of evidence has shown that the hyperinflammatory state, lower production of type I IFN, and altered functions of macrophages and neutrophils contribute to immune dysfunction in the elderly. However, the mechanisms that underlie this phenomenon have yet to be fully elucidated.

Recent studies have revealed that small extracellular vesicles (EVs) mediate intercellular communications and influence our immune system (Kouwaki et al., 2017b; Robbins and Morelli, 2014). Aging and senescence have been found to modulate EV function, but it remains unclear whether aging affects EV-mediated immune regulation. EVs consisting of 30- to 150-nm lipid bilayer vesicles are the potent systemically circulating factors that regulate immune responses, including inflammation (Colombo et al., 2014; Robbins and Morelli, 2014). These vesicles are secreted by many types of cells throughout the body for local or remote cell-to-cell communication, and they contain functional proteins and RNAs, such as microRNAs (miRNAs), which modulate cellular responses. Because of their lipid origins, EVs are readily engulfed by many different types of cells (Alexander et al., 2015; Valadi et al., 2007). Recent studies have shown that EVs deliver several immune regulatory miRNAs suited to different tasks. EV miR-155 enhances pro-inflammatory cytokine expression, and EV miR-146a attenuates inflammatory responses (Alexander et al., 2015). Circulating EVs deliver these immune regulatory miRNAs to DCs and macrophages and can fine-tune inflammatory responses (Alexander et al., 2015). We recently reported that circulating EVs with immune regulatory miRNAs control the inflammatory response of macrophages upon stimulation with the WVP, which is used for vaccination against seasonal flu (Okamoto et al., 2018), suggesting that circulating EVs also participate in the immune response to vaccines. We found that circulating EVs contained high concentration of immune regulatory miRNAs whose levels were correlated to local inflammation at the vaccination site (Miyashita et al., 2019).

In this study, we established an aging mouse model wherein aged mice exhibited lower vaccination efficacy than young mice and identified miR-192, an aging-associated miRNA present in EVs. Interestingly, circulating aging-associated EVs were crucial to the regulation of immune responses to vaccines. Our experiments indicated that the aging-associated EV miR-192 attenuated the hyperinflammatory state and improved vaccine efficacy in geriatric mice. These observations suggest a mechanism of EV-mediated control of immune dysfunction in aging.

RESULTS

miR-192 Is an Aging-Associated miRNA in Circulating EVs

We compared miRNA profiles in serum EVs derived from young (2–3 months) and aged (14–18 months) mice to uncover aging-associated immune regulatory miRNAs in circulating EVs. Total RNAs were extracted from serum EVs of wild-type (WT), IL-6 knockout (KO), and IL-6 receptor (IL6R) KO mice Tsukamoto et al., 2017, and these were subjected to high throughput RNA sequencing (RNA-seq) analysis (Figure 1A). RNA-seq analysis revealed 15 miRNAs whose expression was specifically increased in aged WT mouse serum EVs (Figure 1B). We performed RT-qPCR to confirm our RNA-seq data and found that miR-19b, miR-322, miR-192, miR-21, and miR-181c levels in serum EVs were significantly increased in aged WT mice (Figure 1C). As some of other miRNAs were not detectable in RT-qPCR, we do not exclude the possibility that other miRNAs also increased with aging.

Next, we investigated whether the aging-associated miRNAs regulate the cytokine expression. Mimic RNA for each miRNA was transfected into RAW264.7 cells, and the effect on the cytokine expression in response to a TLR ligand was investigated. Interestingly miR-192 reduced *Il6* and *Ccl2* mRNA levels (Figure 1D). To further clarify this point, we performed microarray analysis and found that miR-192 changed the expression of cytokines, and gene ontology and pathway analyses suggested that miR-192 was related to immune system process and cytokine signaling pathway (Figures S1A–S1C). These data imply that miR-192 plays a role in regulating cytokine responses, and thus we focused on the role of miR-192.

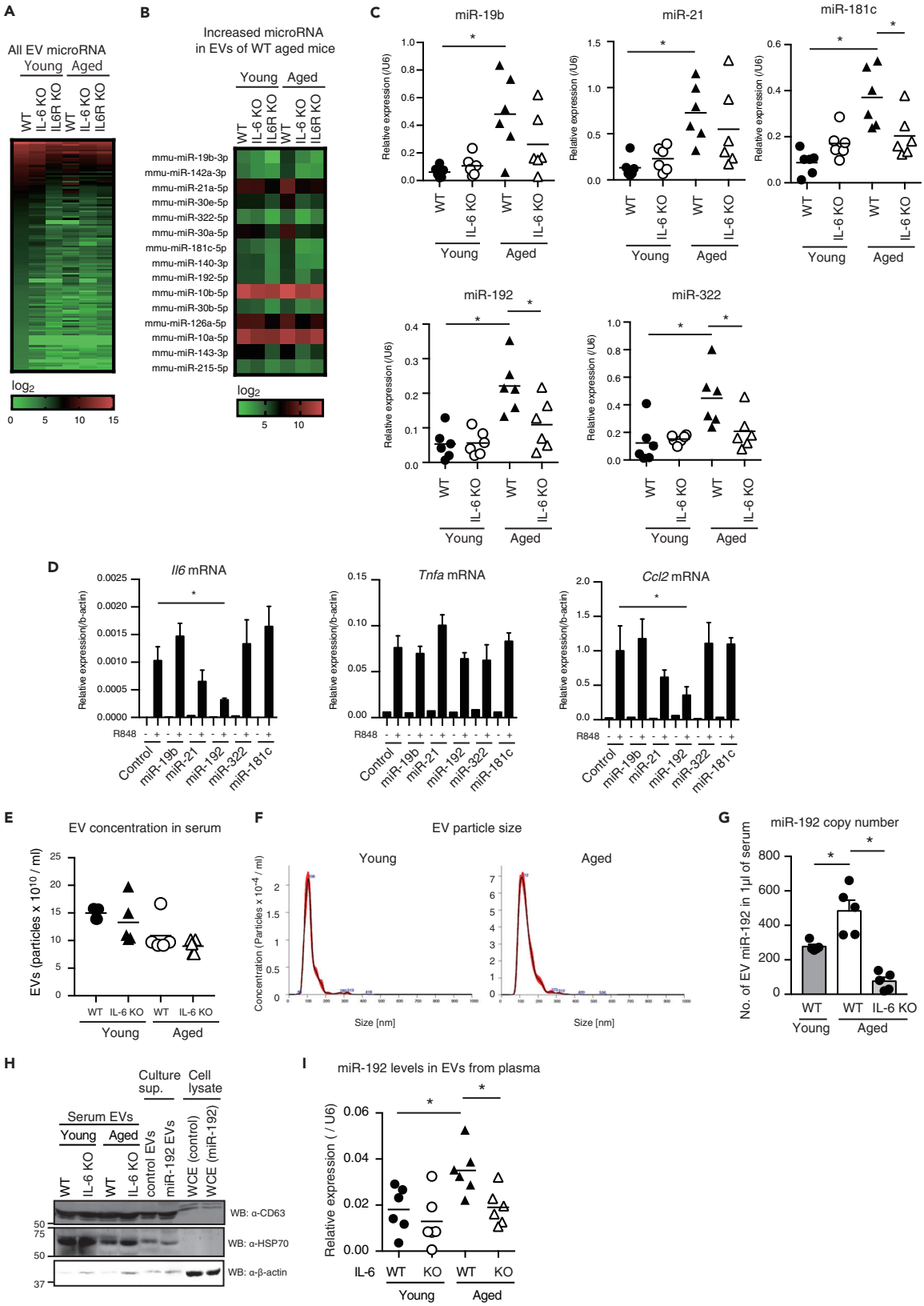
A
All EV microRNA
Young Aged
WT IL-6 KO IL6R KO WT IL-6 KO IL6R KO
log2
0 5 10 15
B
Increased microRNA
in EVs of WT aged mice
Young Aged
WT IL-6 KO IL6R KO WT IL-6 KO IL6R KO
mmu-miR-19b-3p
mmu-miR-142a-3p
mmu-miR-21a-5p
mmu-miR-30e-5p
mmu-miR-322-5p
mmu-miR-30a-5p
mmu-miR-181c-5p
mmu-miR-140-3p
mmu-miR-192-5p
mmu-miR-10b-5p
mmu-miR-30b-5p
mmu-miR-126a-5p
mmu-miR-10a-5p
mmu-miR-143-3p
mmu-miR-215-5p
log2
5 10
C
miR-19b
miR-21
miR-181c
miR-192
miR-322
Relative expression (/U6)
WT IL-6 KO WT IL-6 KO
Young Aged
D
Il6 mRNA
Tnfa mRNA
Ccl2 mRNA
Relative expression/(b-actin)
R848
Control miR-19b miR-21 miR-192 miR-322 miR-181c
E
EV concentration in serum
EVs (particles x 10^10 / ml)
WT IL-6 KO WT IL-6 KO
Young Aged
F
EV particle size
Young
Aged
Concentration (Particles x 10^-4 / ml)
Size [nm]
G
miR-192 copy number
No. of EV miR-192 in 1µl of serum
WT WT IL-6 KO
Young Aged
H
Culture sup.
Cell lysate
Serum EVs
Young Aged
WT IL-6 KO WT IL-6 KO
control EVs
miR-192 EVs
WCE (control)
WCE (miR-192)
WB: α-CD63
WB: α-HSP70
WB: α-β-actin
50
75
50
37
I
miR-192 levels in EVs from plasma
Relative expression (/ U6)
IL-6 WT KO WT KO
Young Aged

Figure 1. Age-Associated miRNAs in EVs

(A and B) RNAs were isolated from serum EVs of five young and aged WT, IL-6 KO, and IL6R KO mice and mixed in each group. Expression profiles of miRNAs in the pooled RNA were assessed by RNA-seq analysis (A). miRNAs with higher expression levels in aged WT mice than those in young WT mice are shown in (B) (heatmap).

(C) Serum EVs were isolated from young and aged WT and IL-6 KO mice (n = 6), and RNA was extracted from isolated EVs. The expression of indicated miRNA levels was determined by RT-qPCR. *$p < 0.05$.

(D) RAW264.7 cells were transfected with indicated miRNA mimic RNA; 36 h after transfection, cells were stimulated with R848, and mRNA expressions of *Il6*, *Tnfa*, and *Ccl2* were determined by RT-qPCR (*$p < 0.05$; n = 3).

(E and F) Concentrations (E) and sizes of EVs (F) in young and aged sera as determined by a NanoSight NS300.

(G) Absolute copy number of EV miR-192 as determined by RT-qPCR (*$p < 0.05$; n = 5).

(H) CD63, Hsp70, and β-actin in EVs collected from sera and culture supernatant and those of whole-cell extracts were detected by western blotting with indicated Abs.

(I) EVs were collected from plasma of young and aged WT and IL-6 KO mice (n = 6). Total RNA was extracted from EVs, and miR-192 levels were determined by RT-qPCR. *$p < 0.05$. Data represent means ± SEM.

See also Figure S1.

Concentrations of serum EVs in aged mice were comparable with those in young mice (Figure 1E). Sizes of collected EVs were around 50–200 nm, which include both exosomes and microvesicles, and no significant difference in diameters was observed between young and elderly mice (Figure 1F). Absolute copy number of miR-192 in EVs was significantly increased in aged mice (Figure 1G). We confirmed that collected EVs expressed CD63 and Hsp70, which are exosome markers (Figure 1H). Increased miR-192 levels in EVs of aged mice were also observed when EVs were collected from the plasma with anti-CD9, CD81, and CD63 antibodies (Abs), which are the markers of the exosomes (Figure 1I).

Next, we sought to uncover the mechanism underlying the increase of miR-192 in aged EVs. As pro-inflammatory cytokines are well-known to be related to aging, we investigated the effect of pro-inflammatory cytokines on the expression of miR-192. Administration of anti-IL-6 antibody (Ab), but neither anti-tumor necrosis factor (TNF)-α nor -IL-1β Ab, reduced serum EV miR-192 levels of aged mice (Figure 2A). Conversely recombinant IL-6, but neither TNF-α nor IL-1β, increased serum EV miR-192 levels in young mice (Figure 2B). In addition, IL-6 KO reduced serum EV miR-192 levels in aged mice (Figures 1C, 1G, and 1I). As previously reported Pinti et al., 2016, serum IL-6 levels in aged mice were higher than those in young mice (Figure 2C), and aged IL-6 KO mice presented with reduced levels of miR-192 comparable with those of normal young mice (Figure 1C), implicating IL-6 signaling in the increase in miR-192 observed in aged EVs. Intravenous administration of IL-6 transiently increased serum IL-6 levels and led to the increase of miR-192 levels in the serum EVs of young mice at 2 days post-IL-6 injection (Figures 2D and 2E), whereas EV miR-192 was not further increased in aged mice due to their constitutively higher level of IL-6 (Figure 2E). These data indicate that elevated IL-6 concentration causes the increase of miR-192 levels in serum EVs. It is possible that the decrease of serum IL-6 level at 2 days (Figure 2D) was caused by absorption and/or degradation of injected IL-6.

As macrophages are the potent regulators of inflammatory response, we assessed their contribution to the increased miR-192 in EVs. Depletion of macrophages with anti-colony-stimulating factor 1 receptor (CSF-1R) Ab significantly reduced the levels of serum EV miR-192 in aged mice (Figure 2F), suggesting that macrophages are responsible for the increase of miR-192 levels in serum EVs *in vivo*.

In contrast to *in vivo* situation, IL-6 alone failed to increase miR-192 levels in EVs released from macrophages *in vitro*, but co-stimulation with R848, a TLR7 ligand, increased EV miR-192 levels (Figures 2G and 2H). Although CL097 or poly I:C alone failed to increase EV miR-192 levels, LPS stimulation increased miR-192 levels released from macrophages (Figure 2H). These observations imply that some kinds of stimulation with PAMPs and/or damage-associated molecular patterns, such as DNA/RNA released from host cells, are required for IL-6 to increase serum EV miR-192 levels *in vivo*. We do not exclude the possibility that R848 or LPS stimulation increased miR-192 levels in EVs through regulating the sensitivity to IL-6.

EV miR-192 Attenuates Pro-inflammatory Cytokine Expression

As miR-192 has the ability to suppress the cytokine expression in response to a TLR ligand (Figure 1D), we next focused on determining its activity. Bone-marrow-derived macrophages (BMMs) were transfected with miR-192 mimic RNA and then stimulated with TLR ligands, such as LPS, R848, CL097, and poly I:C. Interestingly, miR-192 mimic RNA significantly reduced the expression of *Il6* and *Ccl2* in response to

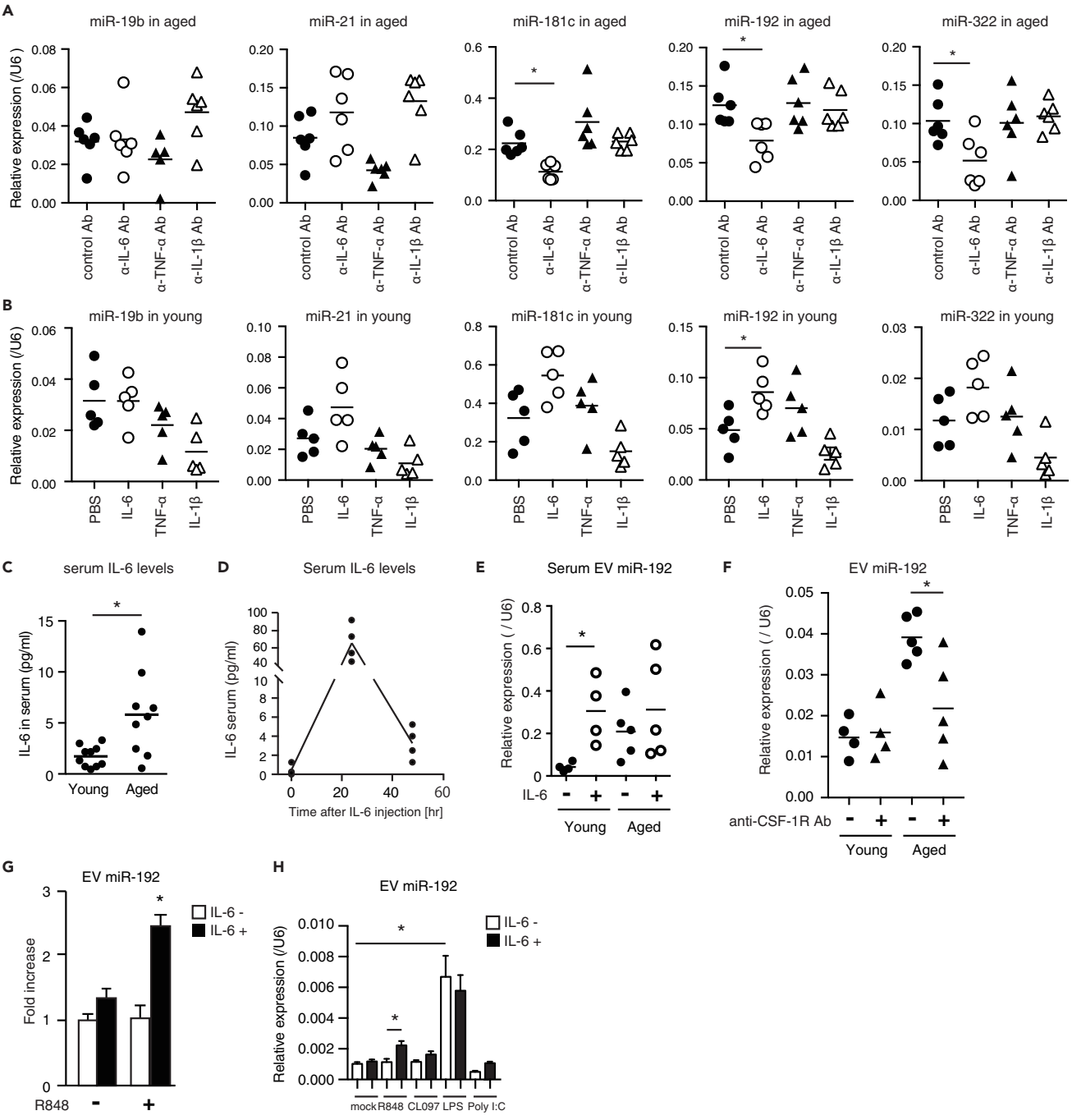

Figure 2. IL-6 Affects EV miR-192 Levels

(A) Control Ab or indicated Abs were injected into aged mice 1 and 3 days before serum harvest. EV miRNA levels were determined by RT-qPCR (*$p < 0.05$; $n = 6$).

(B) Indicated recombinant proteins were intravenously injected into young mice; 2 days after injection, sera were collected, and EV miRNA levels were determined by RT-qPCR (*$p < 0.05$; $n = 6$).

(C) Serum IL-6 levels in young and aged mice as determined by ELISA (*$p < 0.05$; $n = 10$).

(D) IL-6 was injected into young mice ($n = 4$). One and 2 days after injection, sera were collected at indicated time points, and serum IL-6 levels were determined by ELISA ($n = 4$).

(E) IL-6 was injected into young and aged WT mice; 2 days after injection, serum EV miR-192 levels were assessed by RT-qPCR (*$p < 0.05$; $n = 4$ or 5).

(F) Anti-CSF-1R was injected 5 and 2 days before EVs were collected from mouse sera. miR-192 levels in EVs were assessed by RT-qPCR (*$p < 0.05$; $n = 4$ or 5).

Figure 2. *Continued*

(G) Splenic CD11b$^+$ cells were collected using MACS column and stimulated with R848 in the presence or absence of IL-6 (300 ng/mL) for 1 day. EVs were collected from the cell culture medium, and miR-192 levels in EVs were assessed by RT-qPCR (*$p < 0.05$; $n = 5$).

(H) BMMs were stimulated with mock, R848, CL097, LPS, and poly I:C in the presence and absence of 200 ng/mL of IL-6 for 48 h. EVs were collected from cell culture supernatant, and miR-192 levels in EVs were determined by RT-qPCR (*$p < 0.05$; $n = 3$). Data represent means ± SEM.

LPS, R848, and CL097 (Figure 3A). Microarray analysis for miR-192-regulating gene expression profile in LPS-stimulated macrophages revealed that the expressions of several cytokines and chemokines were reduced by miR-192 (Figure 3B). These results were confirmed by RT-qPCR (Figure 3C). As anti-IL-6 Ab did not affect the suppression by miR-192 (Figure 3B), our data weakened the possibility that miR-192-mediated suppression of the cytokine expression was caused by reduced IL-6 expression. In general, a single miRNA targets multiple genes, and our microarray data showed that expression levels of over 100 genes were changed at least 2-fold by miR-192 (Figure S1). Time course analysis also confirmed that miR-192 attenuated the expression of *Il6* and *Ccl2* after R848 stimulation in both mouse RAW264.7 and human CD14$^+$ monocyte-derived macrophages (Figures 3D and 3E). The effect on *Tnfa* expression was modest (Figure 3D). The IL-6 production associated with CL097 and R848 stimulation was reduced by miR-192 (Figures 3F and 3G). These data indicate that miR-192 suppresses the expression of several pro-inflammatory cytokines and chemokines.

It is well known that EVs deliver miRNAs to recipient cells, as demonstrated in macrophages treated with EVs that contained fluorescence-labeled RNA (Figure 3H). Thus, we next investigated whether miR-192 enclosed in EVs could exhibit the same effect as miR-192 itself did. To prepare EVs that contain miR-192 (miR-192 EVs), control mimic or miR-192 mimic RNAs were transfected into RAW264.7 cells and EVs were collected from culture supernatants (Figure S2). CD11b$^+$ Gr1$^-$ macrophages were treated with collected EVs and then stimulated with R848. miR-192 EVs significantly increased intracellular miR-192 levels in macrophages but not the levels of other miRNAs, such as miR-101c (negative control) (Figure 3I). Interestingly, although control EVs tended to down-regulate *Il6* expression with unknown mechanism, miR-192 EVs further reduced the *Il6* and *Il1b* mRNA expression and the IL-6 protein production after R848 stimulation (Figures 3I and 3J). In addition, after LPS intraperitoneal injection, serum IL-6 levels were reduced by intravenous injection of miR-192 EV (Figure 3K). miR-192 EVs reduced serum IL-6 levels even in aged mice stimulated with LPS (Figure 3L). These data suggest that EVs deliver miR-192 to recipient cells, thereby reducing IL-6 production both *in vitro* and *in vivo*.

Because miR-192 levels were increased in aged EVs, we next investigated the effect of aged EVs on IL-6 expression in macrophages. Although young EVs collected from sera did not affect *Il6* expression in macrophages stimulated with R848, aged EVs significantly reduced *Il6* expression (Figure 3M). The expression of *Ccl2* was also reduced by aged EVs (Figure 3M). We assessed the properties of endogenous miR-192 in aged EVs by transfecting antagomir-192 RNA, an inhibitory RNA for miR-192 (anti-miR-192), into macrophages to suppress miR-192 function before treatment with aged EVs. Anti-miR-192, but neither control RNA nor anti-miR-101 (a negative control), negated the effects of aged EVs (Figure 3M). These data indicate that miR-192 enclosed in aged EVs is transferred into macrophages, thereby suppressing the cytokine expression in recipient macrophages.

As those cytokines and chemokines were not predicted to be potential targets by miR-192 in any database, it is possible that miR-192 targets those genes indirectly. We explored this possibility by investigating whether miR-192 targeted the transcription factors for cytokines and chemokines. When cells were transfected with mimic miR-192, degradation of IκB and phosphorylation of p65 and IKKβ caused by R848 stimulation were both reduced (Figure 4A). TBK1 phosphorylation was also reduced by miR-192 (Figure 4A). In contrast, the phosphorylation of ERK and p38 was not affected by miR-192 (Figure 4B). Nuclear localization of nuclear factor (NF)-κB was decreased by miR-192 expression (Figures 4C and 4D). As NF-κB and TBK1 transcription factors induce the expression of *Il6*, *Ccl2*, and *Ifnb*, our data suggest that miR-192 attenuates the expression of pro-inflammatory cytokines and type I IFNs by targeting their transcription factor pathways. Previous studies have reported that miR-192 suppresses ZEB1/2 signaling molecules in epithelial cells and glomerular cells required for pro-inflammatory cytokine expression (Kim et al., 2011; Putta et al., 2012). ZEB2 knockdown reduced *Il6* mRNA expression (Figures S3A and S3B). However, miR-192 failed to reduce ZEB2 protein levels in RAW264.7 cells in our experimental condition (Figure S3A).

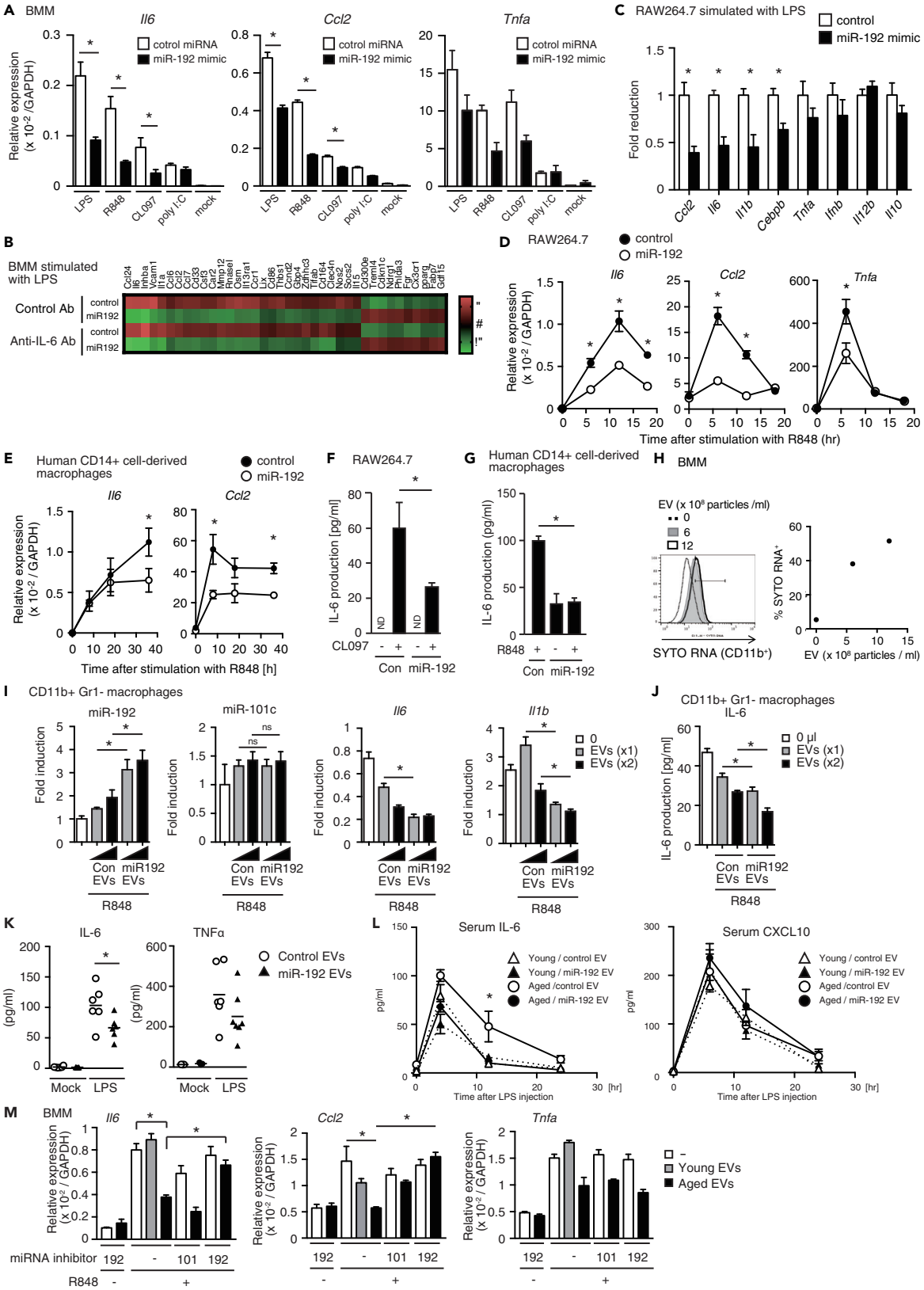
A BMM
Il6
Ccl2
Tnfa
cotrol miRNA
miR-192 mimic
Relative expression (x 10-2 /GAPDH)
LPS
R848
CL097
poly I:C
mock
C RAW264.7 simulated with LPS
control
miR-192 mimic
Fold reduction
Ccl2
Il6
Il1b
Cebpb
Tnfa
Ifnb
Il12b
Il10
B
BMM stimulated with LPS
Control Ab
Anti-IL-6 Ab
control miR192
D RAW264.7
control
miR-192
Relative expression (x 10-2 / GAPDH)
Time after stimulation with R848 (hr)
E Human CD14+ cell-derived macrophages
Time after stimulation with R848 [h]
F RAW264.7
IL-6 production [pg/ml]
ND
CL097
Con
miR-192
G Human CD14+ cell-derived macrophages
IL-6 production (pg/ml)
R848
H BMM
EV (x 10^8 particles /ml)
SYTO RNA (CD11b+)
% SYTO RNA+
EV (x 10^8 particles / ml)
I CD11b+ Gr1- macrophages
miR-192
miR-101c
Il6
Il1b
Fold induction
Con EVs
miR192 EVs
R848
0
EVs (x1)
EVs (x2)
J CD11b+ Gr1- macrophages
IL-6
IL-6 production [pg/ml]
0 µl
EVs (x1)
EVs (x2)
K
IL-6
TNFα
(pg/ml)
Mock
LPS
Control EVs
miR-192 EVs
L
Serum IL-6
Serum CXCL10
pg/ml
Time after LPS injection
Young / control EV
Young / miR-192 EV
Aged /control EV
Aged / miR-192 EV
M BMM
Il6
Ccl2
Tnfa
Relative expression (x 10-2 / GAPDH)
miRNA inhibitor
192
-
101
R848
Young EVs
Aged EVs

Figure 3. miR-192-Enriched EVs Attenuate the Expression of Pro-inflammatory Cytokines

(A) BMMs were transfected with control or miR-192 mimic RNA; 36 h after transfection, cells were stimulated with LPS, R848, CL097, and poly I:C. The expression of *Il6*, *Ccl2*, and *Tnfa* was determined by RT-qPCR (*$p < 0.05$; n = 3).

(B) BMMs were transfected with control or miR-192 mimic RNAs and then were stimulated with LPS for 24 h in the presence of anti-IL6 or control Ab. The heatmap shows the expression profiles of the genes with at least a 2-fold change in expression upon miR-192 mimic RNA transfection in the presence or absence of anti-IL-6 antibody; genes with 1.5-fold changes in expression following anti-IL-6 Ab treatment were removed.

(C–G) RAW264.7 cells and human $CD14^+$ monocyte-derived macrophages were transfected with control and mimic miR-192 RNAs and subsequently stimulated with LPS (C), R848 (D, E, and G), and CL097 (F). The expression of each gene was assessed by RT-qPCR (C, D, and F). The IL-6 protein levels were evaluated by ELISA (F and G) (*$p < 0.05$; n = 3).

(H) RNAs within EVs produced from miR-192-transfected RAW264.7 were labeled with SYTO RNA reagent, which is a membrane-permeable dye transmitting green fluorescence, and added into BMM culture at indicated concentrations. Representative histograms of fluorescent SYTO RNA^+ cells in $CD11b^+CD64^+$ macrophages (left) and their frequencies in each condition (right) are shown.

(I and J) CD11b+ Gr1- macrophages were treated with control or miR-192 EVs (×1, 1 × 10^9 particles, or ×2, 2 × 10^9 particles) collected from 0, 75 (×1), and 150 (×2) μL cell culture supernatants of control- or miR-192-transfected RAW264.7 cells and then were stimulated with R848. The expression levels of miR-192, miR-101c, *Il6*, and *Il1b* were assessed by RT-qPCR (I). IL-6 protein levels in cell culture medium as determined by ELISA (J) (*$p < 0.05$; n = 3).

(K and L) Control and miR-192 EVs were intravenously administrated into young (K and L) and aged mice (L). LPS (2.5 μg/mouse) was injected intraperitoneally into EV-treated young and aged mice, and serum IL-6, TNF-α, and CXCL10 protein levels were assessed by ELISA (*$p < 0.05$; n = 6).

(M) Inhibitor RNAs for miR-192 and miR-101 were transfected into BMMs. Cells were treated with EVs (3 × 10^9 particles) collected from young and aged sera and subsequently stimulated with R848. Expression levels of *Il6*, *Ccl2*, and *Tnfa* were assessed by RT-qPCR (*$p < 0.05$; n = 3). Data represent means ± SEM. See also Figure S2.

EV miR-192 Constitutes a Negative Feedback Loop in Aging-Associated Hyperinflammatory State

Circulating EVs can regulate immune responses after stimulation with inactivated influenza A virus particles called WVP, which are used for vaccination against flu (Okamoto et al., 2018). Thus, we next focused on the effect of aged EVs containing miR-192 on the immune responses to WVP. First, we compared WVP-induced immune responses between young and aged mice. WVP intranasal inoculation induced a transient and systemic increase in inflammatory cytokines, such as IL-6 and CXCL10, in young mice (Figure 5A). However, the higher levels of IL-6, but not CXCL10, were prolonged in aged mouse sera (Figure 5A). Consistent with higher systemic levels of IL-6 in aged mice inoculated with WVP, local expression levels of *Il6*, *Ccl2, and Il12b* in the lung were also augmented in aged mice at later time points (Figures 5B–5G), suggesting that although WVP induced inflammatory responses locally and systemically in young and old mice alike, these effects were exacerbated in aged animals.

Second, we examined which types of cells are responsible for prolonged pro-inflammatory cytokine expression in aged mice by isolating different types of cells from young and aged mice that were subsequently stimulated with WVP *in vitro*. Significantly higher amounts of IL-6 were produced by $CD11b^+$ $Gr1^-$ macrophages isolated from aged mice when compared with those from young mice, whereas the levels of TNF-α production and CXCL10 production in aged macrophages were lower than those of their young counterparts (Figures 5H–5J). These data suggest that those macrophages are responsible for high IL-6 production in geriatric mice.

Third, we investigated whether aged EVs could control the expression of cytokines upon WVP stimulation in broad immune cell populations. Splenocytes including macrophages, DC, B cell, and T cell populations were treated with young and aged EVs and subsequently stimulated with WVP. Although young EVs reduced IL-6 production by splenocytes, aged EVs did so to a higher degree than young EVs (Figure 5K). In addition, aged EVs suppressed *Il6* expression by macrophages via miR-192 (Figure 3M). These data suggest that aged EVs could attenuate macrophage-mediated pro-inflammatory cytokine expression.

Fourth, we assessed the role of EV miR-192 in immune responses to WVP inoculation. Control and miR-192 EVs were intravenously administered to young and aged mice, and after intranasal inoculation of WVP, the expression levels of miRNAs and cytokines in the lungs of EVs-administrated mice were evaluated. Although the expression levels of *Il6*, *Il12b*, *Tnfa*, *Ifng*, and *Ccl2* after WVP inoculation were higher in aged mice than in young mice 60 h after WVP inoculation, cytokine and chemokine expression levels were significantly reduced by administration of miR-192 EVs (Figure 6A). We confirmed that administration of miR-192 EVs increased miR-192 levels in the lung and those in lung $CD11b^+$ $Gr\text{-}1^-$ macrophages (Figures 6A and 6B). Consistent with the local inflammation, miR-192 EVs also abrogated prolonged systemic

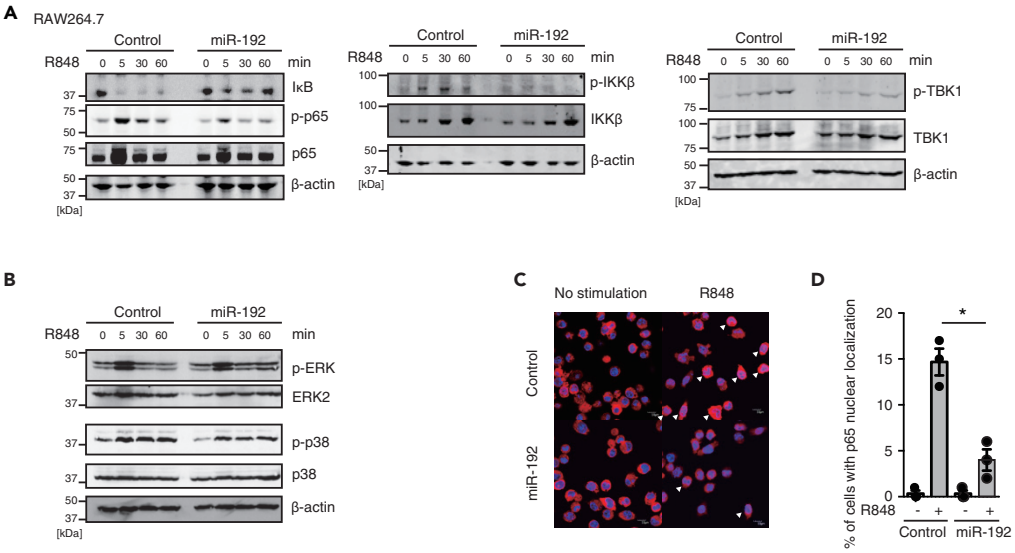

Figure 4. miR-19 Attenuates the Activation of NF-κB and TBK1

(A–D) RAW264.7 cells were transfected with control or miR-192 mimic RNAs and then stimulated with R848. Whole-cell extracts (WCE) were subjected to SDS-PAGE, and the proteins were resolved via western blotting with indicated Abs (A and B). One hour after stimulation with R848, cells were fixed and stained with anti-NF-κB p65 Ab (red) and DAPI (blue), and the subcellular localization was observed with a confocal microscope (C). The percentages of cells with nuclear localization of NF-κB p65 are shown in (D) (*$p < 0.05$; $n = 3$). Data represent means ± SEM.
See also Figure S3.

increase of IL-6 in aged mice (Figure 6C). The population of alveolar macrophages ($F4/80^+$ $CD11c^+$ $SiglecF^+$ cells), which are tissue-resident macrophages, was dramatically decreased by intranasal administration of WVP, whereas WVP induced the recruitment and accumulation of $Ly6C^+$ monocytes and $F4/80^+$ $CD11c^-$ interstitial macrophages, which are differentiated from monocytes, in the lung 60 h after inoculation (Figure 6D). Accumulation and recruitment of interstitial macrophages were more apparent in aged mice (Figures 6D and S4A). miR-192 EVs significantly suppressed recruitment and accumulation of interstitial macrophages in aged mice (Figure 6D). It is possible that miR-192 EV-mediated suppression of *Il12b* and *Tnfa* expression in the lung is due to lower accumulation of interstitial macrophages, because miR-192 failed to efficiently reduce *Il12b* and *Tnfa* expression *in vitro*. Collectively, these data indicate that aged EVs and miR-192 EV could attenuate aging-associated prolonged cytokine expression in response to WVP inoculation *in vitro* and *in vivo*.

Upon depletion with anti-CSF-1R, interstitial macrophages were reduced in the lung after WVP inoculation (Figures S4Band S4C). Interestingly, anti-CSF-1R treatment significantly reduced *Il6* and *Ccl2* mRNA expression in the lung after WVP inoculation (Figure 6E), suggesting that interstitial macrophages are responsible for the expression of *Il6* and *Ccl2* in the lung. In addition, IL-6 protein levels in the BALF were also reduced by anti-CSF-1R Ab treatment (Figure 6F). These data suggest that interstitial macrophages are responsible for the augmented inflammatory responses observed in vaccinated aged mice. These observations also support that miR-192 EVs and aged EVs reduce the cytokine expression in macrophages and attenuate hyperinflammatory state in aged mice. As anti-CSF-1R treatment also reduced the number of splenic macrophages, but not those of dendritic cells, monocytes, and PMN/MDSC in the spleen (Figures 6G and S5A), we do not exclude the possibility that other types of macrophages are involved in miR-192 EV-mediated immune regulation.

To assess the effect of other miRNAs whose expression were increased with aging, we prepared EVs containing miR-19b, miR-21, and miR-322 as miR-192 and assessed the effect on WVP-induced increase of serum IL-6 in aged mice. Interestingly, miR-21 EVs as well as miR-192 EVs suppressed IL-6 levels after WVP administration (Figure 6H). This data implies that not only miR-192 EVs but also other aging-associated EVs, such as miR-21 EVs, contribute to the suppression of age-associated inflammation.

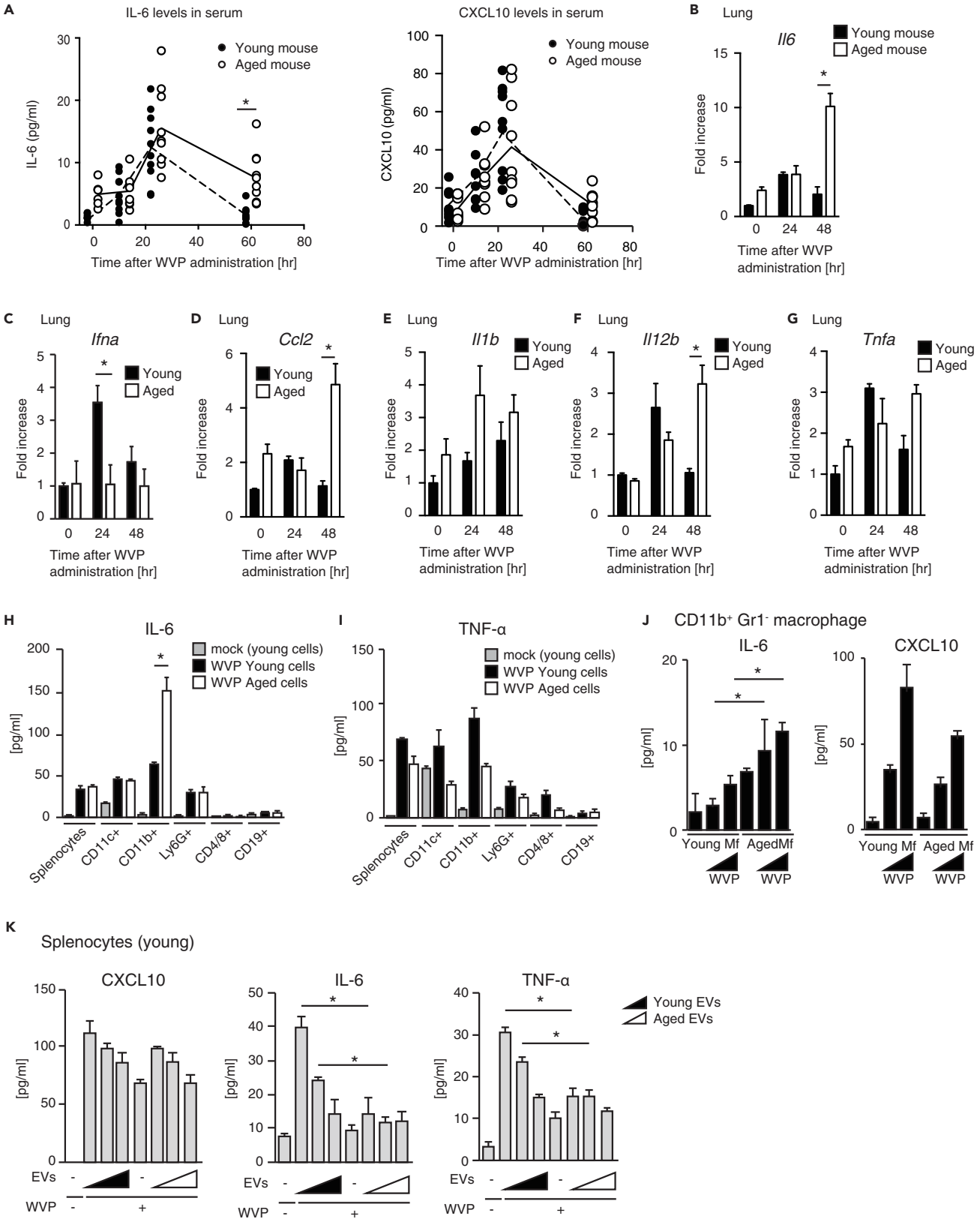
A
IL-6 levels in serum
Young mouse
Aged mouse
IL-6 (pg/ml)
Time after WVP administration [hr]
CXCL10 levels in serum
CXCL10 (pg/ml)
B
Lung
Il6
Fold increase
C
Ifna
D
Ccl2
E
Il1b
F
Il12b
G
Tnfa
Young
Aged
Time after WVP administration [hr]
H
IL-6
mock (young cells)
WVP Young cells
WVP Aged cells
[pg/ml]
Splenocytes
CD11c+
CD11b+
Ly6G+
CD4/8+
CD19+
I
TNF-α
J
CD11b+ Gr1- macrophage
Young Mf
AgedMf
Aged Mf
WVP
K
Splenocytes (young)
EVs
Young EVs
Aged EVs

Figure 5. Aging-Associated Changes in Immune Responses upon Vaccination

(A–G) WVPs were intranasally inoculated into young and aged mice. Serum IL-6 and CXCL10 protein levels were evaluated by ELISA (A) (*$p < 0.05$; n = 9). The mRNA expression levels of *Il6* (B), *Ifna* (C), *Ccl2* (D), *Il1b* (E), *Il12b* (F), and *Tnfa* (G) in the lungs of young and aged mice were assessed by RT-qPCR (*$p < 0.05$; n = 5).

(H and I) Total splenocytes (splenocytes) and splenic CD11c+, CD11b+, Ly6G+, CD4/8+, and CD19+ cells were isolated from young and aged mice. Cells were then stimulated with 2 μg WVP. The IL-6 (H) and TNF-α (I) protein levels in cell culture media were evaluated by ELISA (*$p < 0.05$; n = 3).

(J) Splenic CD11b+ Gr1- macrophages were stimulated with 0, 1, or 2 μg WVP for 36 h, and the IL-6 and CXCL10 levels in the culture media were evaluated by ELISA (*$p < 0.05$; n = 3).

(K) Splenocytes were treated with EVs (1, 3, or 6 × 10^9 particles) collected from young or aged mice and then stimulated with WVP. The CXCL10, IL-6, and TNF-α protein levels were evaluated by ELISA (*$p < 0.05$; n = 4). Data represent means ± SEM.

Effect of miR-192 EVs on Macrophages and Dendritic Cells

Next, we investigated whether miR-192 EVs affected the immune responses to other types of stimulation, that is, LPS-induced peritonitis model. Administration of miR-192 EVs reduced the numbers of total cells and F4/80$^+$ macrophages accumulated in peritoneal lavage fluid in aged mice after LPS stimulation (Figures 7A–7C). Consistent with these, IL-6 level in peritoneal lavage fluid was reduced by miR-192 EV administration (Figure 7D). These data suggest that miR-192 EVs reduce the inflammatory response not only to WVP but also to other types of stimulation, such as LPS in peritonitis model.

To assess the effect of miR-192 EVs on the innate immune response, we investigated whether miR-192 EVs regulate the expression of MHC and co-stimulatory molecules. Stimulation with R848 increased major histocompatibility complex (MHC)-I, MHC-II, and CD86 expression of bone-marrow-derived dendritic cells (BMDCs); however, miR-192 EVs did not change their expression levels in BMDCs stimulated with or without R848 (Figures S6A and S6B). These *in vitro* results were supported by the fact that administration of miR-192 EVs did not affect the expression of MHC-I, MHC-II, and CD86 in CD11c$^+$ DCs from WVP-inoculated aged mice (Figures S6C and S6D). These data suggest that miR-192 EVs attenuate the expression of cytokines but not MHC and CD86 required for antigen presentation.

Therapeutic Potential of Aging-Associated miR-192 EVs to Improve Vaccination Efficacy in the Elderly

Previous studies have shown that excessive inflammation reduced vaccine efficacy (Fourati et al., 2016; Park et al., 2014). Thus, it is expected that aged mice exhibit an attenuated response to WVP. When WVP was inoculated into young and aged mice, antigen-specific total IgG production was significantly reduced in aged mice (Figure 8A). These data indicate that our mouse model reflects reduced vaccine efficacy in elderly mice. Interestingly, IL-6 KO improved the production of specific IgG upon WVP inoculation in aged mice (Figure 8A), suggesting that IL-6-mediated inflammation in aged mice is associated with reduced vaccine efficacy by WVP. Although IL6 KO increased Ab production in aged mice (Figure 8A), IL-6 KO mice were more susceptible to viral infection than wild-type mice even if they were vaccinated (Figure S6E). This is because IL-6 itself plays protective roles during influenza A virus infection (Farsakoglu et al., 2019). These data suggest that appropriate inflammation, but not excessive inflammation, is required for efficient vaccination and protection against viral infection.

As miR-192 EVs regulated pro-inflammatory responses after WVP administration in the lungs of aged mice, we expected that miR-192 EVs would improve the efficacy of vaccination with WVP in aged mice. We tested this possibility by administering control and miR-192 EVs to mice 1 day before vaccination as described in Figure 8B. Vaccinated mice were then infected with influenza A virus, and survival and their body weight loss were recorded. In young mice, vaccination prolonged the survival of virally infected mice, and miR-192 EVs did not affect survival or weight loss after viral infection (Figures 8C and 8D). We confirmed that administration of EVs itself did not affect the protective activity of WVP vaccination (Figure S6F). In aged mice, vaccination exhibited a marginal effect on protection from flu infection (Figure 8C); however, survival of vaccinated aged mice was significantly improved by administration of miR-192 EVs (Figure 8C). These data indicate a therapeutic potential of miR-192 EVs in vaccination of the elderly. When we evaluated the Th1 and Th2 responses in young and aged mice we found that Th1 response, such as IFN-γ expression, was not induced in response to WVP in aged mice, whereas Th2 response, such as IL-5 expression, was induced even in aged mice (Figure S7), suggesting that Th1 response is attenuated in aged mice. Interestingly, specific IgG and IgG2c, but not IgG1, were markedly increased by miR-192 EVs administration into aged mice (Figure 8E). As IgG2c production is known to require Th1 response, these data suggest that

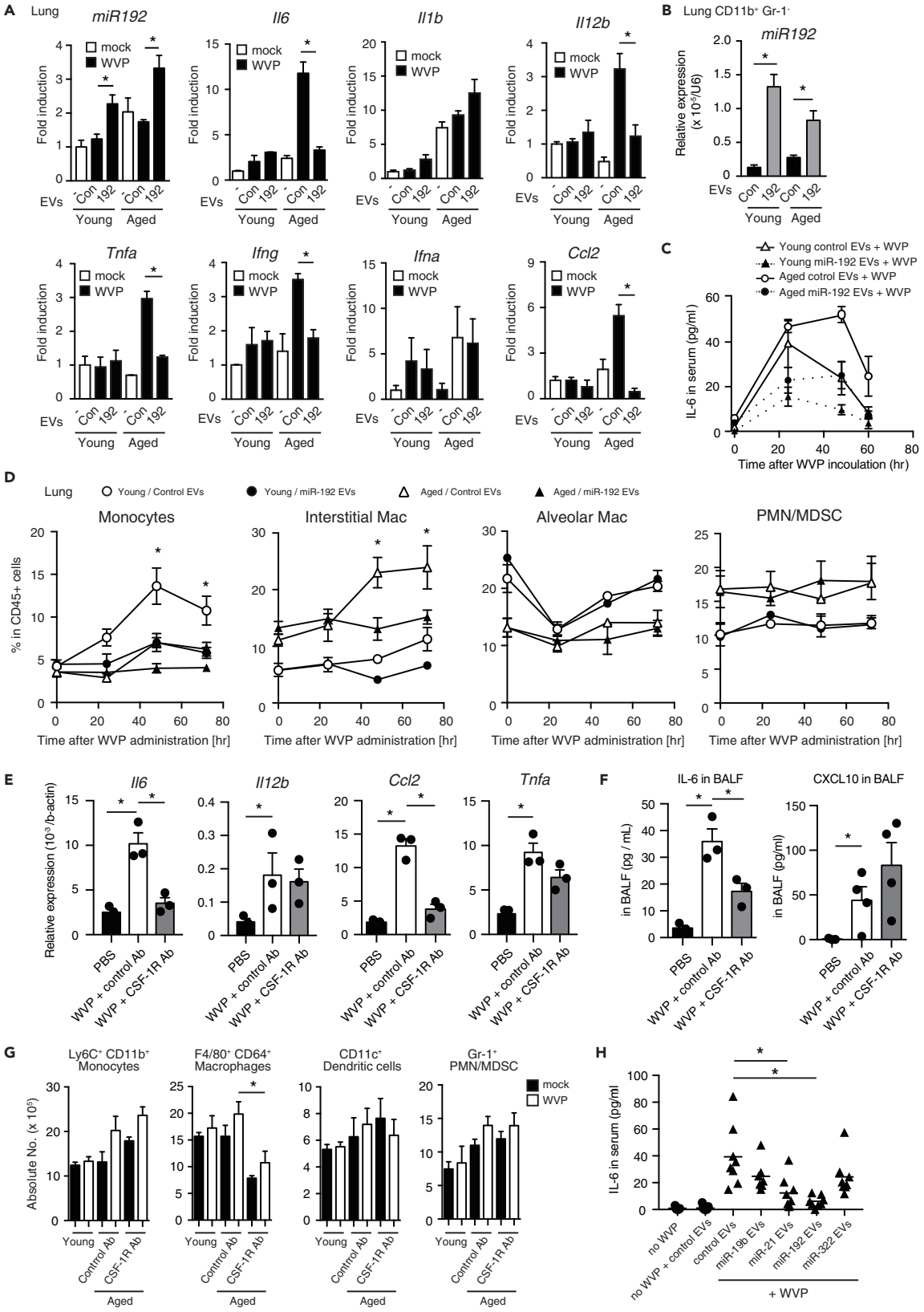
A
Lung
miR192
Il6
Il1b
Il12b
Tnfa
Ifng
Ifna
Ccl2
mock
WVP
Fold induction
EVs
Con
192
Young
Aged
B
Lung CD11b+ Gr-1-
miR192
Relative expression (x 10-5/U6)
C
Young control EVs + WVP
Young miR-192 EVs + WVP
Aged cotrol EVs + WVP
Aged miR-192 EVs + WVP
IL-6 in serum (pg/ml)
Time after WVP incoulation (hr)
D
Lung
Young / Control EVs
Young / miR-192 EVs
Aged / Control EVs
Aged / miR-192 EVs
Monocytes
Interstitial Mac
Alveolar Mac
PMN/MDSC
% in CD45+ cells
Time after WVP administration [hr]
E
Il6
Il12b
Ccl2
Tnfa
Relative expression (10-3/b-actin)
PBS
WVP + control Ab
WVP + CSF-1R Ab
F
IL-6 in BALF
CXCL10 in BALF
in BALF (pg / mL)
in BALF (pg/ml)
G
Ly6C+ CD11b+ Monocytes
F4/80+ CD64+ Macrophages
CD11c+ Dendritic cells
Gr-1+ PMN/MDSC
Absolute No. (x 10^5)
Young
Control Ab
CSF-1R Ab
Aged
H
IL-6 in serum (pg/ml)
no WVP
no WVP + control EVs
control EVs
miR-19b EVs
miR-21 EVs
miR-192 EVs
miR-322 EVs
+ WVP

Figure 6. miR-192 EVs Alleviate Hyperinflammatory State in Aged Mice in Response to WVP

(A–C) Control or miR-192 EVs were intravenously injected into young and aged mice. After 14 h, WVP were intranasally administrated. Expression levels of cytokines, chemokines, and miRNAs in the lung 60 h post-vaccination were assessed by RT-qPCR (A) (n = 5). The levels of miR-192 in $CD11b^{+}$ $Gr\text{-}1^{-}$ myeloid population isolated from lung 30 h after vaccination were assessed by RT-qPCR (B) (n = 4). Serum IL-6 levels at indicated time points were determined by ELISA (n = 5) (C). *p < 0.05.

(D) Control or miR-192 EVs were intravenously injected into young and aged mice. After 14 h, WVP were intranasally administrated. The frequencies of indicated myeloid populations in CD45+ cells in the lung were assessed by flow cytometry (*p < 0.05; n = 5).

(E and F) Aged mice were treated with macrophage-depleting anti-CSF-1R or control Ab three times before and after WVP administration. Two days after WVP administration, indicated gene expression in the lung (E) and protein levels in BALF (F) were assessed by RT-qPCR and ELISA (*p < 0.05; n = 3).

(G) At 0 and 2 days before WVP inoculation, control and anti-CSF-1R Abs were injected into aged mice. Two days after WVP inoculation, indicated population in the spleen was analyzed by flow cytometry. Absolute numbers of indicated populations are shown (*p < 0.05; n = 3).

(H) Indicated miRNA-enriched EVs were transferred into aged mice 18 h before WVP inoculation; 40 h after WVP inoculation, serum IL-6 levels were determined by ELISA (*p < 0.05; n = 5). Data represent means ± SEM.

See also Figures S4 and S6.

miR-192 EVs improved Th1 response in aged mice. This is consistent with the observation that miR-192 EVs improved vaccine efficacy. Taken together, our data indicate that aging-associated EV miR-192 alleviates the hyper-inflammatory state, leading to improved vaccination efficacy.

DISCUSSION

Aging gives rise to pleiotropic effects on our immune system, including inflammatory responses, and a hyperinflammatory state in aged humans and animals, termed as "inflamm-aging," partially accounts for certain age-related immune dysfunction, such as lower vaccine efficacy (Ferrucci and Fabbri, 2018; Franceschi et al., 2000; Pinti et al., 2016). It is thereby critical that we expand our knowledge about how the systemic and local inflammatory responses are modulated in old age. Here, we found that miR-192 levels in circulating EVs were increased in aged mice. Injection of IL-6 into young mice also increased EV miR-192 levels, and a shutdown of IL-6 signaling decreased EV miR-192 levels in aged mice. On the basis of our data, we conclude that the aging-associated hyperinflammatory state, especially increased IL-6 levels in sera, is a cause of increased miR-192 levels in EVs associated with aging.

Aging-associated EV miR-192 decreased the expression of several cytokines and chemokines, such as IL-6 and CCL2. Macrophages released miR-192 EVs, and depletion of macrophages reduced circulating miR-192 EV levels in aged mice, suggesting an autocrine activity of miR-192 EVs in macrophages. IL-6 is a pro-inflammatory cytokine and is known to amplify its expression (Franchimont et al., 1997; Kawano et al., 1988; Lee et al., 2012). Thus, EV miR-192 constitutes autocrine negative feedback regulation to relieve inflammation of aged individuals and buffer aging-associated hyperinflammation. The hyperinflammatory state decreased vaccination efficacy, and miR-192 EVs rescued this efficacy in aged mice. It is possible that increased miR-192 EVs' levels with aging is not sufficient to cancel the aging effect on vaccination, and thus miR-192 EVs' administration increased the efficacy of vaccination. It is expected that this negative feedback loop may help improve vaccination efficacy in elderly humans, as well.

Our microarray data revealed that several miRNA levels in EVs were increased in aged mice. Previous studies have shown that these miRNAs control inflammatory responses. For instance, miR-322 targeted mRNA of NF-κB p50 and attenuated cytokine expression in response to LPS in RAW264.7 cells (Zhang et al., 2017). In addition, miR-181c targeted 3′ UTR region of TLR4 mRNA and downregulated TLR4-mediated expression of TNF-α, IL-1β, and iNOS (Zhang et al., 2015). miR-140-5p also targeted the TLR4/MyD88 axis and alleviated inflammation in the lung injury (Yang et al., 2018). Moreover, miR-30a bound to 3′ UTR region of IRF4, thereby suppressing IL-17-associated autoimmune inflammation (Zhao et al., 2016). As miR-322, miR-181c, miR-140-5p, and miR-30a levels in EVs were increased in aged mice (Figures 1B and 1C), our data suggest that aged EVs contain several anti-inflammatory miRNAs as well as miR-192. Considering that the miR-192 inhibitor canceled the effect of aged EVs on macrophages (Figure 3M), our data indicate that miR-192 plays a role in aged EVs-mediated anti-inflammatory effects. However, we do not exclude the possibility that not only miR-192 but also other immune suppressive miRNAs are required for aged EV-mediated suppression of pro-inflammatory cytokine expression. In general, knockout studies of miRNAs are difficult because of their redundancy (Park et al., 2010). Indeed, it has been reported that there are several miR-192-encoding loci (Lim et al., 2003). Knockout of miR-192 as well as other miRNAs might be useful to further reveal the role of aging-associated EVs.

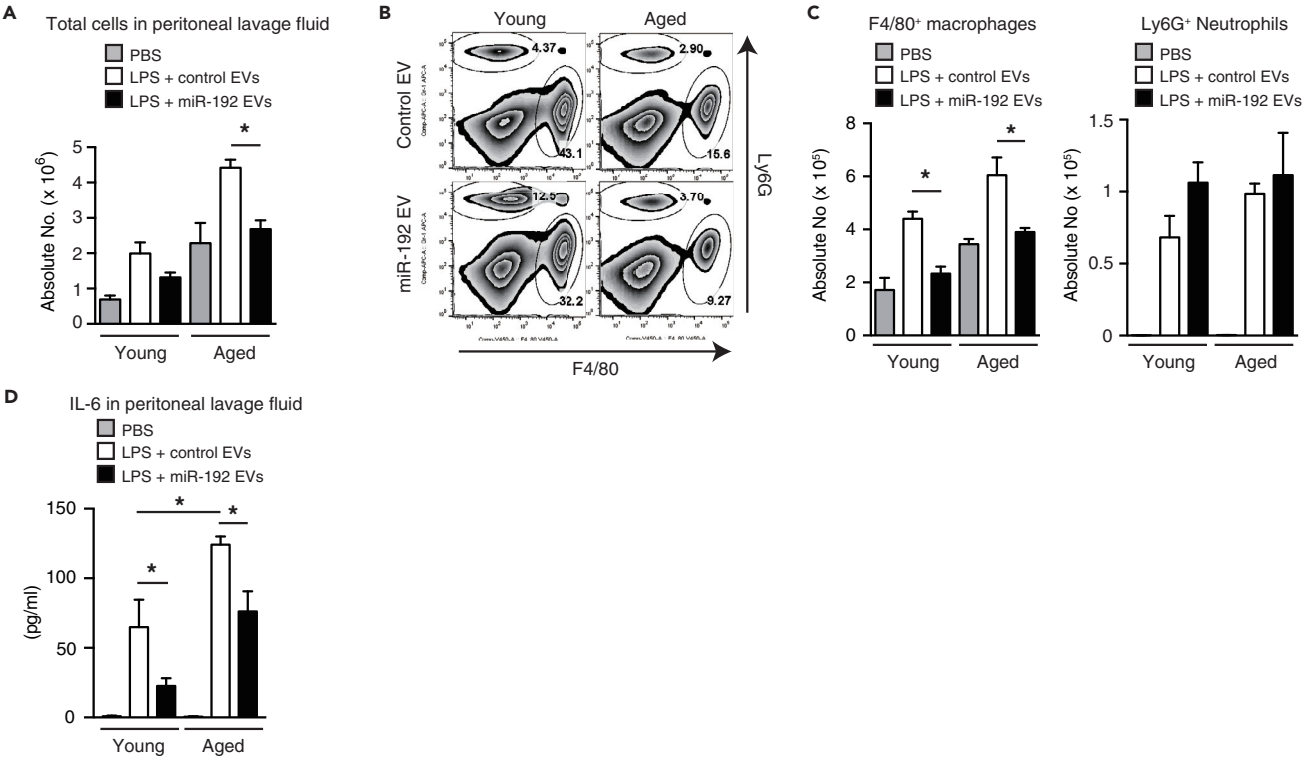

Figure 7. miR-192 EVs Regulate the Cytokine Expression in Macrophages

(A–D) Young and aged mice were intravenously administrated with control miRNA EVs or miR-192 EVs. Twenty four hours after administration, mice were intraperitoneally injected with LPS. Cells were collected from peritoneal lavage fluid 4 h after LPS injections. Total cell number in peritoneal lavage fluid (A), representative plots for F4/80$^+$ macrophages and Ly6G$^+$ neutrophils (B), absolute numbers of macrophages (C left) and neutrophils (C right), and IL-6 concentration (D) in peritoneal lavage fluid are shown. Data represent means ± SEM with n = 3 or 4; *p < 0.05.

See also Figure S6.

Many host factors have been reported to contribute to the aging-associated immunological abnormalities such as severe adverse events in vaccinated aged individuals (Gouin et al., 2008). However, it remains unclear which of these phenomena should be targeted to ameliorate the pathogenic features of inflammation. Here, we showed that miR-192 EVs were associated with attenuated inflammatory responses and improved vaccine efficacy in aged mice. This finding is consistent with the theory that excessive inflammation diminishes vaccination efficacy (Fourati et al., 2016; Park et al., 2014). Considering that macrophages have strong phagocytotic activity and that the priming of naive T cells is mainly mediated by DCs *in vivo* (Jung et al., 2002; Mempel et al., 2004), accumulation of macrophages in the lung could lead to WVP digestion and clearance of antigens, resulting in the reduced uptake of antigens by DCs necessary for the priming of naive T cells. Our study elucidated a therapeutic potential for miR-192 EVs wherein they could be used to control harmful inflammation and improve vaccine efficacy in the elderly.

miR-192 itself has pleiotropic functions. Previous studies have shown that the p53 protein regulates the expression of miR-192 and that miR-192 represses ZEB1 and ZEB2 expression (Kim et al., 2011; Putta et al., 2012). The ZEB1/2 proteins induce the expression of pro-inflammatory cytokine, such as IL-6 (Katsura et al., 2017). In this study, we found that miR-192 attenuated the activation of NF-κB. As NF-κB and ZEB1/2 are both inducers of pro-inflammatory cytokines and chemokines, we prefer the interpretation that miR-192 regulates the activation of these transcription factors, resulting in the attenuated expression of pro-inflammatory cytokines and chemokines. miR-192 EVs constitute a negative feedback loop via IL-6; however, TNF-α or IL-12 was not largely involved in the loop. Further studies are required to uncover the detailed mechanism underlying miR-192-mediated selective regulation of inflammation.

Increases in circulating miR-192 levels have also been reported in nonalcoholic fatty liver disease, hepatocellular carcinoma caused by hepatitis B virus, and patients with adenocarcinoma (Pirola et al., 2015; Song

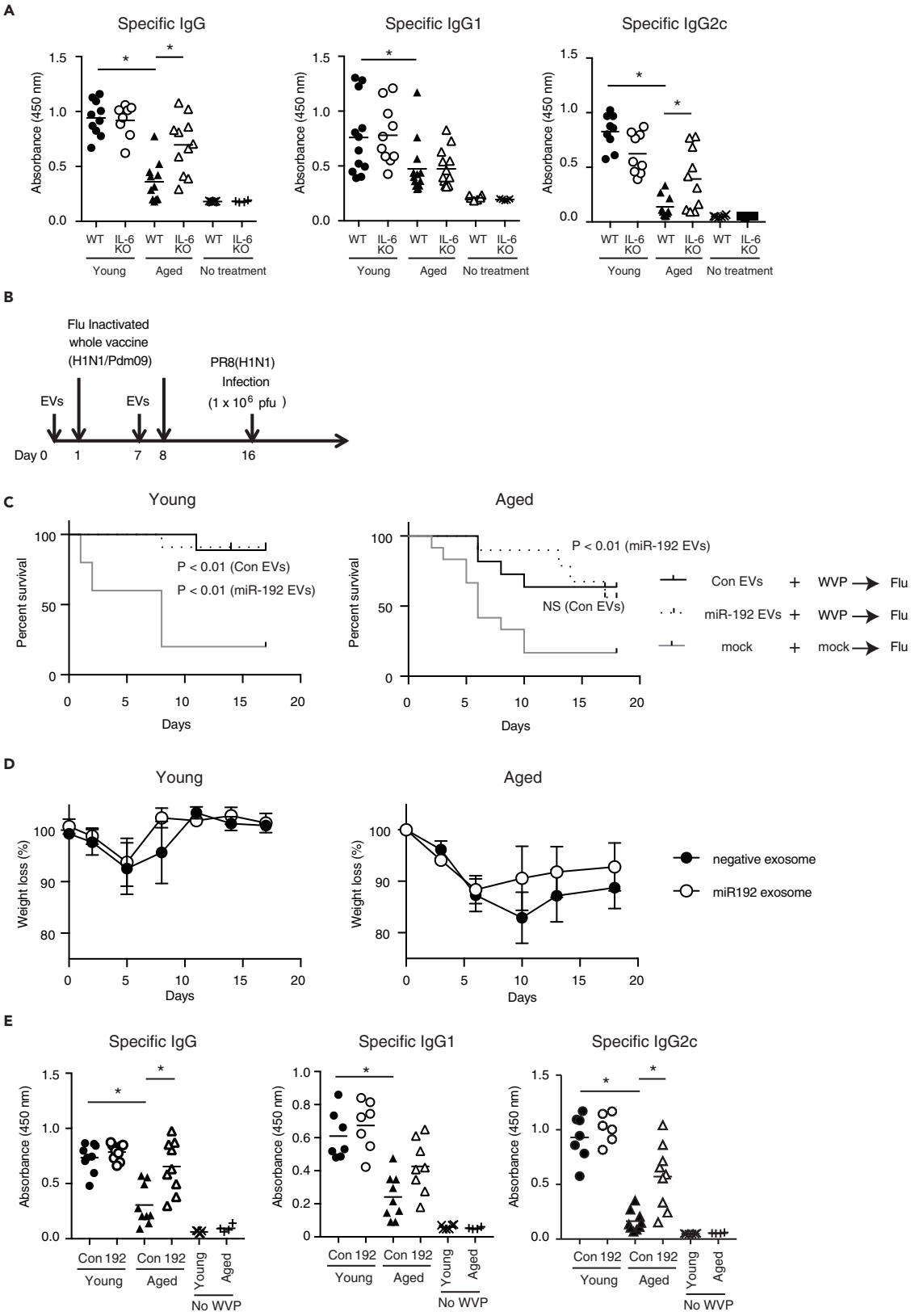
A
Specific IgG
Specific IgG1
Specific IgG2c
Absorbance (450 nm)
WT
IL-6 KO
Young
Aged
No treatment
B
Flu Inactivated whole vaccine (H1N1/Pdm09)
PR8(H1N1) Infection (1 x 10^6 pfu)
EVs
Day 0
1
7
8
16
C
Young
Aged
Percent survival
Days
P < 0.01 (Con EVs)
P < 0.01 (miR-192 EVs)
NS (Con EVs)
Con EVs + WVP → Flu
miR-192 EVs + WVP → Flu
mock + mock → Flu
D
Weight loss (%)
negative exosome
miR192 exosome
E
Con 192
No WVP

Figure 8. miR-192 EVs Improve Flu Vaccine Efficacy in Aged Mice

(A) WVP were intranasally administrated twice into WT and IL-6 KO mice. After 14 days, antigen-specific total IgG, IgG1, and IgG2c levels in sera were assessed (*$p < 0.05$; $n = 10$).

(B) Schedule of treatment with EVs and vaccination with WVP.

(C and D) Control and miR-192 EVs were injected into young and aged mice before WVP administration as shown in (A). Mice were then infected with influenza A virus (PR8). Mouse survival (C) and body weights of survived mice (D) were recorded. Non-vaccinated (mock) versus control EV-treated aged groups (Con EV), $p > 0.01$ (Log rank test). Mock versus miR-192-enriched EV-treated aged groups (miR-192 EV), $p < 0.01$ (log rank test) ($n = 10–12$).

(E) Control and miR-192 EVs were injected into young and aged mice 1 day before vaccination with WVP. Abs were used to assess IgG, IgG1, and IgG2 (*$p < 0.05$; $n = 6–8$). Data represent means ± SEM.

See also Figure S7.

et al., 2012; Zhou et al., 2011). These diseases are associated with inflammation, and thus it is expected that an increase of miR-192 levels in EVs might be instigated by an inflammatory state not only in the elderly but also in young individuals with inflammatory diseases. It would be interesting to test whether the negative feedback loop constituted by miR-192 EVs alleviates inflammation and immune dysfunctions in these patients in the future. Recent studies reported that cellular senescence is controlled by EVs. Senescence affects the levels of an IFN-stimulated protein, IFITM3, in EVs that induces paracrine senescence, resulting in the upregulation of IFITM and downregulation of the chemokine, IL-8 (Borghesan et al., 2019). Cellular senescence is also associated with aging, and here we showed that aged EVs could downregulate pro-inflammatory cytokines. These observations indicate that circulating EVs participate in aging-associated changes in the immune system.

Limitations of the Study

This study proposes that the EVs from aged B6 mice and their components including miR-192 have immuno-modulating ability to suppress inflammatory response in macrophages in the mouse model. On the other hand, it is also important to acknowledge an incomplete understanding in their *in vivo* role and specific effects on immune cells other than macrophages and DC, especially in humans. It is possible that immune-modulating properties of EVs are heavily affected by their cellular sources, recipient tissue microenvironment, and hosts' baseline immunity including genetic differences. Mechanistically, cellular context-dependent target gene(s) of miR-192 are yet to be fully determined, which might be an obstacle for comprehensive understanding of the aging-associated immune defects *in vivo*. These limitations should be further resolved for future translational applications utilizing the microRNA-containing EVs.

Resource Availability

Lead Contact

Further information and requests for resources should be directed to and will be fulfilled by the Lead Contact, Hiroyuki Oshiumi (oshiumi@kumamoto-u.ac.jp).

Materials Availability

This study did not generate new unique materials.

Data and Code Availability

All data produced or analyzed for this study are included in the published article and its supplementary information files. The accession numbers for the RNA-seq data and for the microarray data reported in this paper are DRA009054 in DDBJ database and GSE138758 in GEO, respectively.

METHODS

All methods can be found in the accompanying Transparent Methods supplemental file.

SUPPLEMENTAL INFORMATION

Supplemental Information can be found online at https://doi.org/10.1016/j.isci.2020.101520.

ACKNOWLEDGMENT

We thank Maiko Takahashi (Kamakura Techno-Science Inc.) for her invaluable assistance with 3D-Gene analyses and all our laboratory members for technical assistant and helpful discussion. This work was supported in part by Grants-in-Aid from the Ministry of Education, Science and Technology (MEXT), Japan

Agency for Medical Research and Development (AMED), JSPS KAKENHI No. 18K07325, the Takeda Science Foundation, and the Kumamoto University Advance Research Project A "International Research Center for Cancer and Metabolism".

AUTHOR CONTRIBUTIONS

H.T. and H.O. designed experiments. T.K. performed flu infection assay, and H.T. performed all other experiments. H.T. and H.O. wrote the manuscript. All authors read and approved the final manuscript.

DECLARATION OF INTERESTS

The authors declare no competing interests.

Received: February 18, 2020
Revised: June 30, 2020
Accepted: August 27, 2020
Published: September 25, 2020

REFERENCES

Akira, S., Uematsu, S., and Takeuchi, O. (2006). Pathogen recognition and innate immunity. Cell *124*, 783–801.

Alexander, M., Hu, R., Runtsch, M.C., Kagele, D.A., Mosbruger, T.L., Tolmachova, T., Seabra, M.C., Round, J.L., Ward, D.M., and O'Connell, R.M. (2015). Exosome-delivered microRNAs modulate the inflammatory response to endotoxin. Nat. Commun. *6*, 7321.

Banchereau, J., Briere, F., Caux, C., Davoust, J., Lebecque, S., Liu, Y.J., Pulendran, B., and Palucka, K. (2000). Immunobiology of dendritic cells. Annu. Rev. Immunol. *18*, 767–811.

Borghesan, M., Fafian-Labora, J., Eleftheriadou, O., Carpintero-Fernandez, P., Paez-Ribes, M., Vizcay-Barrena, G., Swisa, A., Kolodkin-Gal, D., Ximenez-Embun, P., Lowe, R., et al. (2019). Small extracellular vesicles are key regulators of non-cell autonomous intercellular communication in senescence via the interferon protein IFITM3. Cell Rep. *27*, 3956–3971 e3956.

Brodin, P., Jojic, V., Gao, T., Bhattacharya, S., Angel, C.J., Furman, D., Shen-Orr, S., Dekker, C.L., Swan, G.E., Butte, A.J., et al. (2015). Variation in the human immune system is largely driven by non-heritable influences. Cell *160*, 37–47.

Colombo, M., Raposo, G., and Thery, C. (2014). Biogenesis, secretion, and intercellular interactions of exosomes and other extracellular vesicles. Annu. Rev. Cell Dev. Biol. *30*, 255–289.

Dalod, M., Chelbi, R., Malissen, B., and Lawrence, T. (2014). Dendritic cell maturation: functional specialization through signaling specificity and transcriptional programming. EMBO J. *33*, 1104–1116.

Diebold, S.S., Kaisho, T., Hemmi, H., Akira, S., and Reis e Sousa, C. (2004). Innate antiviral responses by means of TLR7-mediated recognition of single-stranded RNA. Science *303*, 1529–1531.

Farsakoglu, Y., Palomino-Segura, M., Latino, I., Zanaga, S., Chatziandreou, N., Pizzagalli, D.U., Rinaldi, A., Bolis, M., Sallusto, F., Stein, J.V., et al. (2019). Influenza vaccination induces NK-Cell-Mediated type-II IFN response that regulates humoral immunity in an IL-6-dependent manner. Cell Rep *26*, 2307–2315 e2305.

Ferrucci, L., and Fabbri, E. (2018). Inflammageing: chronic inflammation in ageing, cardiovascular disease, and frailty. Nat. Rev. Cardiol. *15*, 505–522.

Fourati, S., Cristescu, R., Loboda, A., Talla, A., Filali, A., Railkar, R., Schaeffer, A.K., Favre, D., Gagnon, D., Peretz, Y., et al. (2016). Pre-vaccination inflammation and B-cell signalling predict age-related hyporesponse to hepatitis B vaccination. Nat. Commun. *7*, 10369.

Franceschi, C., Bonafe, M., Valensin, S., Olivieri, F., De Luca, M., Ottaviani, E., and De Benedictis, G. (2000). Inflamm-aging. An evolutionary perspective on immunosenescence. Ann. N. Y. Acad. Sci. *908*, 244–254.

Franchimont, N., Rydziel, S., and Canalis, E. (1997). Interleukin 6 is autoregulated by transcriptional mechanisms in cultures of rat osteoblastic cells. J. Clin. Invest. *100*, 1797–1803.

Fulop, T., Le Page, A., Fortin, C., Witkowski, J.M., Dupuis, G., and Larbi, A. (2014). Cellular signaling in the aging immune system. Curr. Opin. Immunol. *29*, 105–111.

Garcon, N., Chomez, P., and Van Mechelen, M. (2007). GlaxoSmithKline Adjuvant Systems in vaccines: concepts, achievements and perspectives. Expert Rev. Vaccines *6*, 723–739.

Gomez, C.R., Boehmer, E.D., and Kovacs, E.J. (2005). The aging innate immune system. Curr. Opin. Immunol. *17*, 457–462.

Gouin, J.P., Hantsoo, L., and Kiecolt-Glaser, J.K. (2008). Immune dysregulation and chronic stress among older adults: a review. Neuroimmunomodulation *15*, 251–259.

Hemmi, H., Kaisho, T., Takeuchi, O., Sato, S., Sanjo, H., Hoshino, K., Horiuchi, T., Tomizawa, H., Takeda, K., and Akira, S. (2002). Small anti-viral compounds activate immune cells via the TLR7 MyD88-dependent signaling pathway. Nat. Immunol. *3*, 196–200.

Jung, S., Unutmaz, D., Wong, P., Sano, G., De los Santos, K., Sparwasser, T., Wu, S., Vuthoori, S., Ko, K., Zavala, F., et al. (2002). In vivo depletion of CD11c+ dendritic cells abrogates priming of CD8+ T cells by exogenous cell-associated antigens. Immunity *17*, 211–220.

Katsura, A., Tamura, Y., Hokari, S., Harada, M., Morikawa, M., Sakurai, T., Takahashi, K., Mizutani, A., Nishida, J., Yokoyama, Y., et al. (2017). ZEB1-regulated inflammatory phenotype in breast cancer cells. Mol. Oncol. *11*, 1241–1262.

Kawai, T., and Akira, S. (2011). Toll-like receptors and their crosstalk with other innate receptors in infection and immunity. Immunity *34*, 637–650.

Kawano, M., Hirano, T., Matsuda, T., Taga, T., Horii, Y., Iwato, K., Asaoku, H., Tang, B., Tanabe, O., Tanaka, H., et al. (1988). Autocrine generation and requirement of BSF-2/IL-6 for human multiple myelomas. Nature *332*, 83–85.

Kim, T., Veronese, A., Pichiorri, F., Lee, T.J., Jeon, Y.J., Volinia, S., Pineau, P., Marchio, A., Palatini, J., Suh, S.S., et al. (2011). p53 regulates epithelial-mesenchymal transition through microRNAs targeting ZEB1 and ZEB2. J. Exp. Med. *208*, 875–883.

Kouwaki, T., Okamoto, M., Tsukamoto, H., Fukushima, Y., and Oshiumi, H. (2017b). Extracellular vesicles deliver host and virus RNA and regulate innate immune response. Int. J. Mol. Sci. *18*, 666.

Koyama, S., Aoshi, T., Tanimoto, T., Kumagai, Y., Kobiyama, K., Tougan, T., Sakurai, K., Coban, C., Horii, T., Akira, S., et al. (2010). Plasmacytoid dendritic cells delineate immunogenicity of influenza vaccine subtypes. Sci. Transl. Med. *2*, 25ra24.

Lee, J., Nakagiri, T., Oto, T., Harada, M., Morii, E., Shintani, Y., Inoue, M., Iwakura, Y., Miyoshi, S., Okumura, M., et al. (2012). IL-6 amplifier, NF-kappaB-triggered positive feedback for IL-6 signaling, in grafts is involved in allogeneic rejection responses. J. Immunol. *189*, 1928–1936.

Lim, L.P., Glasner, M.E., Yekta, S., Burge, C.B., and Bartel, D.P. (2003). Vertebrate microRNA genes. Science *299*, 1540.

Medzhitov, R., Preston-Hurlburt, P., and Janeway, C.A., Jr. (1997). A human homologue of the Drosophila Toll protein signals activation of adaptive immunity. Nature *388*, 394–397.

Mempel, T.R., Henrickson, S.E., and Von Andrian, U.H. (2004). T-cell priming by dendritic cells in lymph nodes occurs in three distinct phases. Nature *427*, 154–159.

Miyashita, Y., Ishikawa, K., Fukushima, Y., Kouwaki, T., Nakamura, K., and Oshiumi, H. (2019). Immune-regulatory microRNA expression levels within circulating extracellular vesicles correspond with the appearance of local symptoms after seasonal flu vaccination. PLoS One *14*, e0219510.

Molony, R.D., Nguyen, J.T., Kong, Y., Montgomery, R.R., Shaw, A.C., and Iwasaki, A. (2017). Aging impairs both primary and secondary RIG-I signaling for interferon induction in human monocytes. Sci. Signal. *10*, eaan2392.

Okamoto, M., Fukushima, Y., Kouwaki, T., Daito, T., Kohara, M., Kida, H., and Oshiumi, H. (2018). MicroRNA-451a in extracellular, blood-resident vesicles attenuates macrophage and dendritic cell responses to influenza whole-virus vaccine. J. Biol. Chem. *293*, 18585–18600.

Park, C.Y., Choi, Y.S., and McManus, M.T. (2010). Analysis of microRNA knockouts in mice. Hum. Mol. Genet. *19*, R169–R175.

Park, H.L., Shim, S.H., Lee, E.Y., Cho, W., Park, S., Jeon, H.J., Ahn, S.Y., Kim, H., and Nam, J.H. (2014). Obesity-induced chronic inflammation is associated with the reduced efficacy of influenza vaccine. Hum. Vaccin. Immunother. *10*, 1181–1186.

Peiris, J.S., Cheung, C.Y., Leung, C.Y., and Nicholls, J.M. (2009). Innate immune responses to influenza A H5N1: friend or foe? Trends Immunol. *30*, 574–584.

Pinti, M., Appay, V., Campisi, J., Frasca, D., Fulop, T., Sauce, D., Larbi, A., Weinberger, B., and Cossarizza, A. (2016). Aging of the immune system: focus on inflammation and vaccination. Eur. J. Immunol. *46*, 2286–2301.

Pirola, C.J., Fernandez Gianotti, T., Castano, G.O., Mallardi, P., San Martino, J., Mora Gonzalez Lopez Ledesma, M., Flichman, D., Mirshahi, F., Sanyal, A.J., and Sookoian, S. (2015). Circulating microRNA signature in non-alcoholic fatty liver disease: from serum non-coding RNAs to liver histology and disease pathogenesis. Gut *64*, 800–812.

Putta, S., Lanting, L., Sun, G., Lawson, G., Kato, M., and Natarajan, R. (2012). Inhibiting microRNA-192 ameliorates renal fibrosis in diabetic nephropathy. J. Am. Soc. Nephrol. *23*, 458–469.

Robbins, P.D., and Morelli, A.E. (2014). Regulation of immune responses by extracellular vesicles. Nat. Rev. Immunol. *14*, 195–208.

Rose-John, S., Winthrop, K., and Calabrese, L. (2017). The role of IL-6 in host defence against infections: immunobiology and clinical implications. Nat. Rev. Rheumatol. *13*, 399–409.

Song, J., Bai, Z., Han, W., Zhang, J., Meng, H., Bi, J., Ma, X., Han, S., and Zhang, Z. (2012). Identification of suitable reference genes for qPCR analysis of serum microRNA in gastric cancer patients. Dig. Dis. Sci. *57*, 897–904.

Tsukamoto, H., Fujieda, K., Hirayama, M., Ikeda, T., Yuno, A., Matsumura, K., Fukuma, D., Araki, K., Mizuta, H., Nakayama, H., et al. (2017). Soluble IL6R expressed by myeloid cells reduces tumor-specific Th1 differentiation and drives tumor progression. Cancer Res. *77*, 2279–2291.

Valadi, H., Ekstrom, K., Bossios, A., Sjostrand, M., Lee, J.J., and Lotvall, J.O. (2007). Exosome-mediated transfer of mRNAs and microRNAs is a novel mechanism of genetic exchange between cells. Nat. Cell Biol. *9*, 654–659.

Wang, Z., Zhang, A., Wan, Y., Liu, X., Qiu, C., Xi, X., Ren, Y., Wang, J., Dong, Y., Bao, M., et al. (2014). Early hypercytokinemia is associated with interferon-induced transmembrane protein-3 dysfunction and predictive of fatal H7N9 infection. Proc. Natl. Acad. Sci. U S A *111*, 769–774.

Yang, Y., Liu, D., Xi, Y., Li, J., Liu, B., and Li, J. (2018). Upregulation of miRNA-140-5p inhibits inflammatory cytokines in acute lung injury through the MyD88/NF-kappaB signaling pathway by targeting TLR4. Exp. Ther. Med. *16*, 3913–3920.

Zhang, L., Li, Y.J., Wu, X.Y., Hong, Z., and Wei, W.S. (2015). MicroRNA-181c negatively regulates the inflammatory response in oxygen-glucose-deprived microglia by targeting Toll-like receptor 4. J. Neurochem. *132*, 713–723.

Zhao, M., Sun, D., Guan, Y., Wang, Z., Sang, D., Liu, M., Pu, Y., Fang, X., Wang, D., Huang, A., et al. (2016). Disulfiram and diphenhydramine hydrochloride upregulate miR-30a to suppress IL-17-associated autoimmune inflammation. J. Neurosci. *36*, 9253–9266.

Zhang, K., Song, F., Lu, X., Chen, W., Huang, C., Li, L., Liang, D., Cao, S., and Dai, H. (2017). MicroRNA-322 inhibits inflammatory cytokine expression and promotes cell proliferation in LPS-stimulated murine macrophages by targeting NF-kappaB1 (p50). Biosci. Rep. *37*, BSR20160239.

Zhou, J., Yu, L., Gao, X., Hu, J., Wang, J., Dai, Z., Wang, J.F., Zhang, Z., Lu, S., Huang, X., et al. (2011). Plasma microRNA panel to diagnose hepatitis B virus-related hepatocellular carcinoma. J. Clin. Oncol. *29*, 4781–4788.

iScience, Volume *23*

Supplemental Information

Aging-Associated Extracellular Vesicles Contain Immune Regulatory microRNAs Alleviating Hyperinflammatory State and Immune Dysfunction in the Elderly

Hirotake Tsukamoto, Takahisa Kouwaki, and Hiroyuki Oshiumi

Supplemental Figures

Figure S1. Microarray of miR-192 transfected macrophages, Related Figure 1.

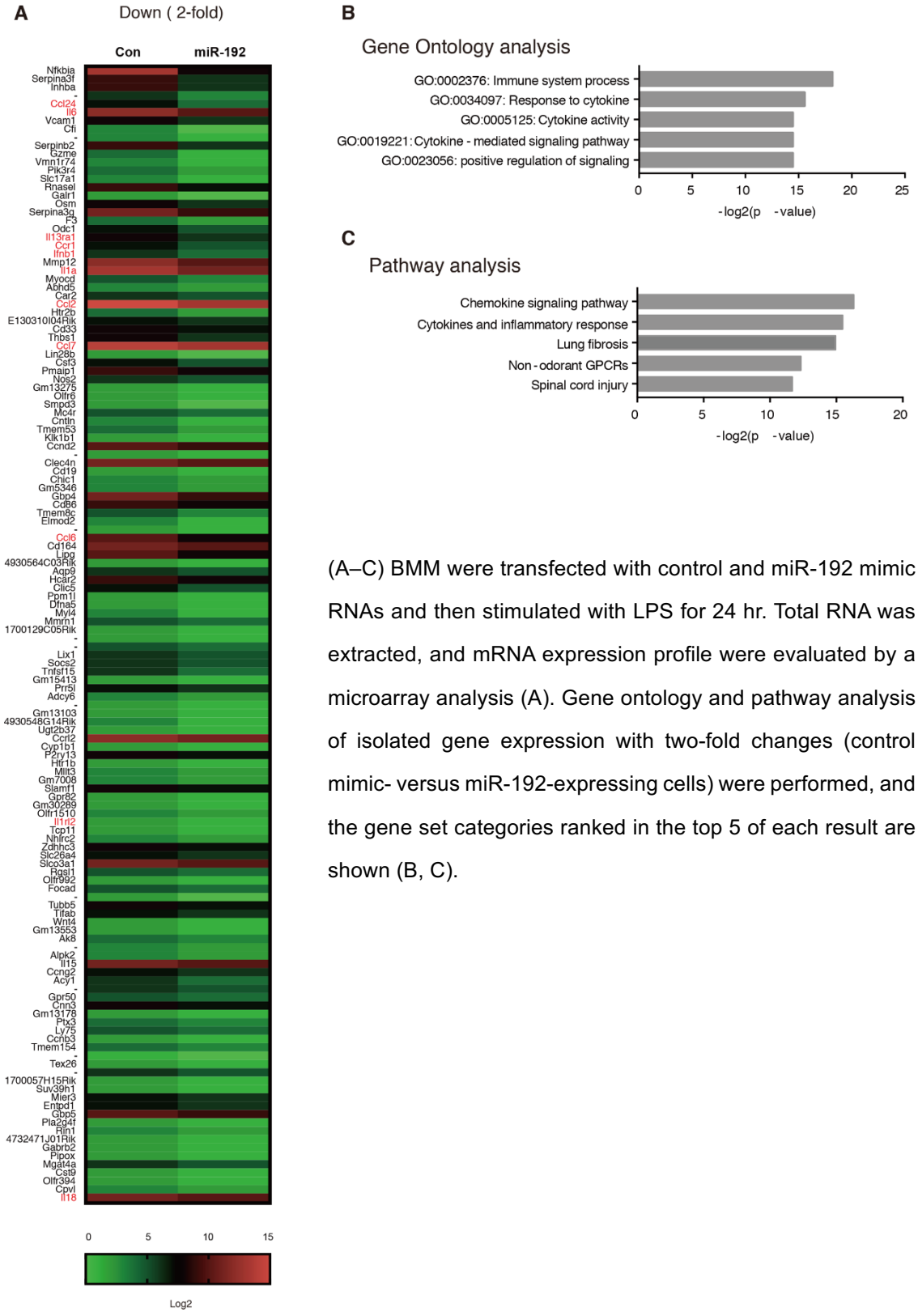

(A–C) BMM were transfected with control and miR-192 mimic RNAs and then stimulated with LPS for 24 hr. Total RNA was extracted, and mRNA expression profile were evaluated by a microarray analysis (A). Gene ontology and pathway analysis of isolated gene expression with two-fold changes (control mimic- versus miR-192-expressing cells) were performed, and the gene set categories ranked in the top 5 of each result are shown (B, C).

Figure S2. Nanoparticle tracking analysis (NTA) of EVs isolated from miR mimic-transfected RAW264.7 cells, Related to Figure 3.

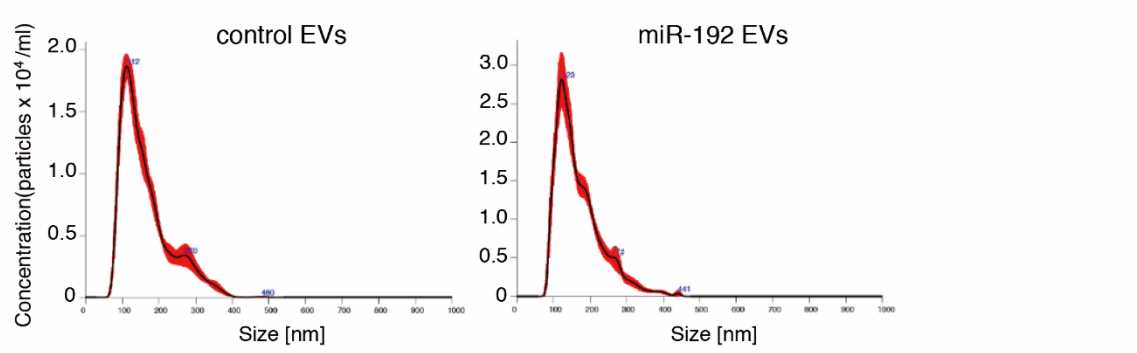

Representatives of NTA of EVs produced by control mimic (left) or miR-192 (right)-transfected RAW264.7 cells are shown.

Figure S3. ZEB2 and miR-192 expression, Related Figure 4.

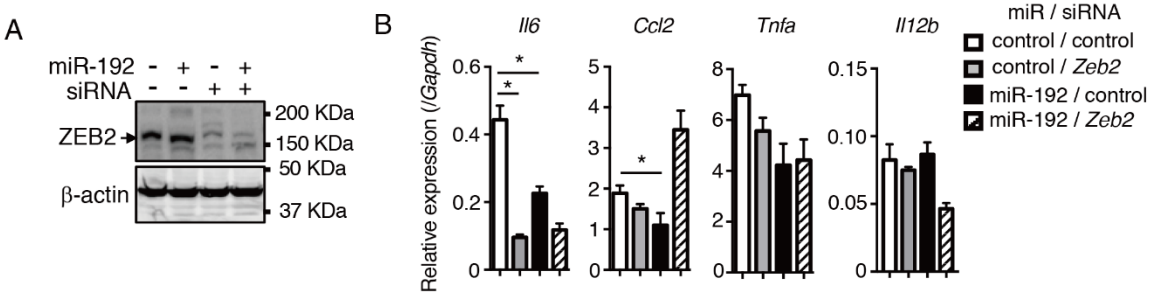

(A) miR-192 mimic RNA and siRNA for ZEB2 were transfected into RAW264.7 cells. 2 days after transfection, cell lysates were prepared and were subjected to SDS-PAGE. The proteins were detected by indicated Abs. (B) Control miRNA, miR-192 mimic RNA, and siRNAs for control and ZEB2 were transfected into RAW264.7 cells as indicated. Two days after transfections, cells were stimulated with R848, and the expression of *Il6*, *Ccl2*, *Tnfa*, and *Il12b* was determined by RT-qPCR (*$p < 0.05$; n = 3). Data represent means ± SEM.

Figure S4. Inflammatory response and population of myeloid cells in miR-192 EVs- and WVP-treated mice, Related Figure 6.

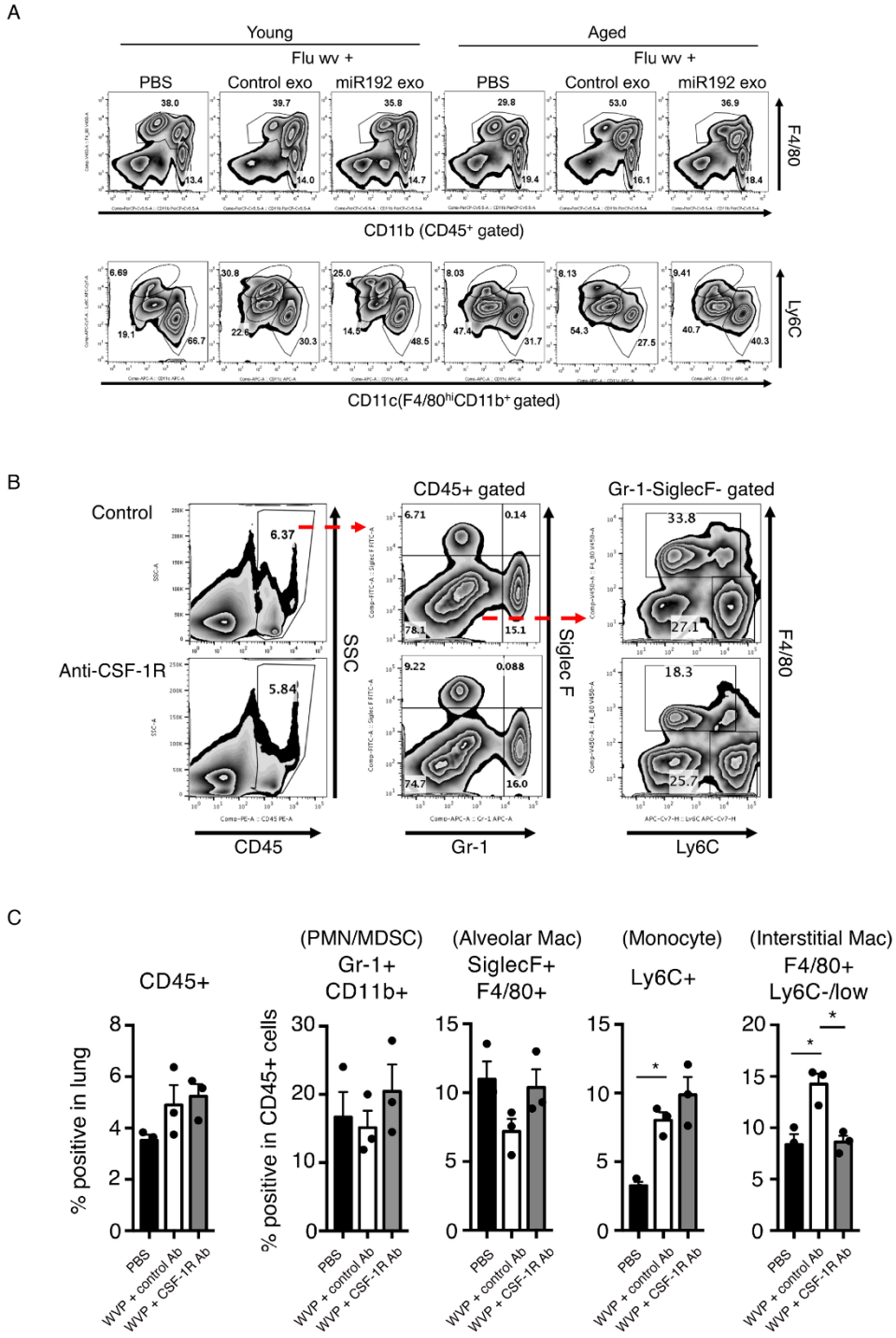

(A–C) Following administration of EVs (A) or injection of anti-CSF-1R Ab (B) into young and aged mice, WVP were intranasally administrated as shown in Figure 6. Indicated myeloid populations in CD45$^+$ cells in the lung were analyzed by flow cytometry. Gating strategy and representative plots from young (A) and aged (A, B) mice are shown. The frequencies of each myeloid population from individual aged mice are summarized in (C) (*$p < 0.05$; n = 3). Data represent means ± SEM.

Figure S5. Representative plots of cell populations in the spleen, Related to Figure 6.

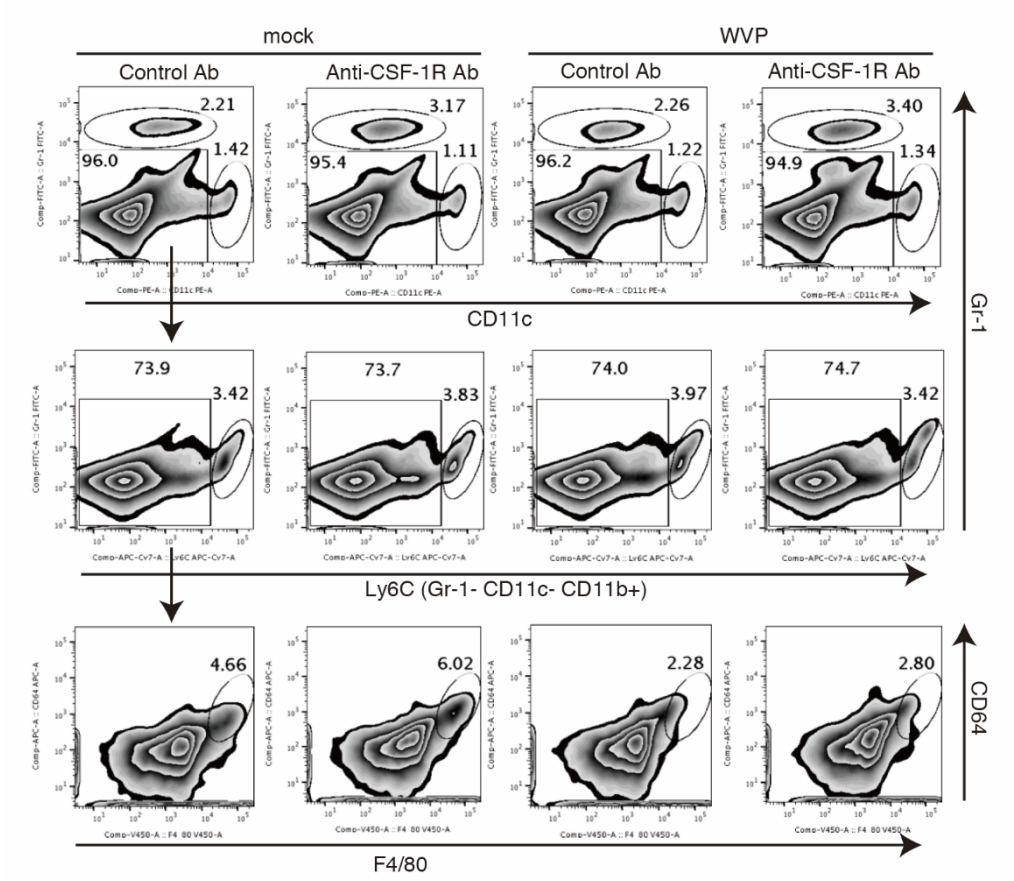

Aged mice were inoculated with WVP. Two days later, indicated populations in the spleen were analyzed. Anti-CSF-1R or control Ab were injected twice (2 days before and at WVP inoculation). Representative plots of indicated populations are shown.

Figure S6. Effect of miR-192 EVs on the innate immune responses, Related to Figure 7.

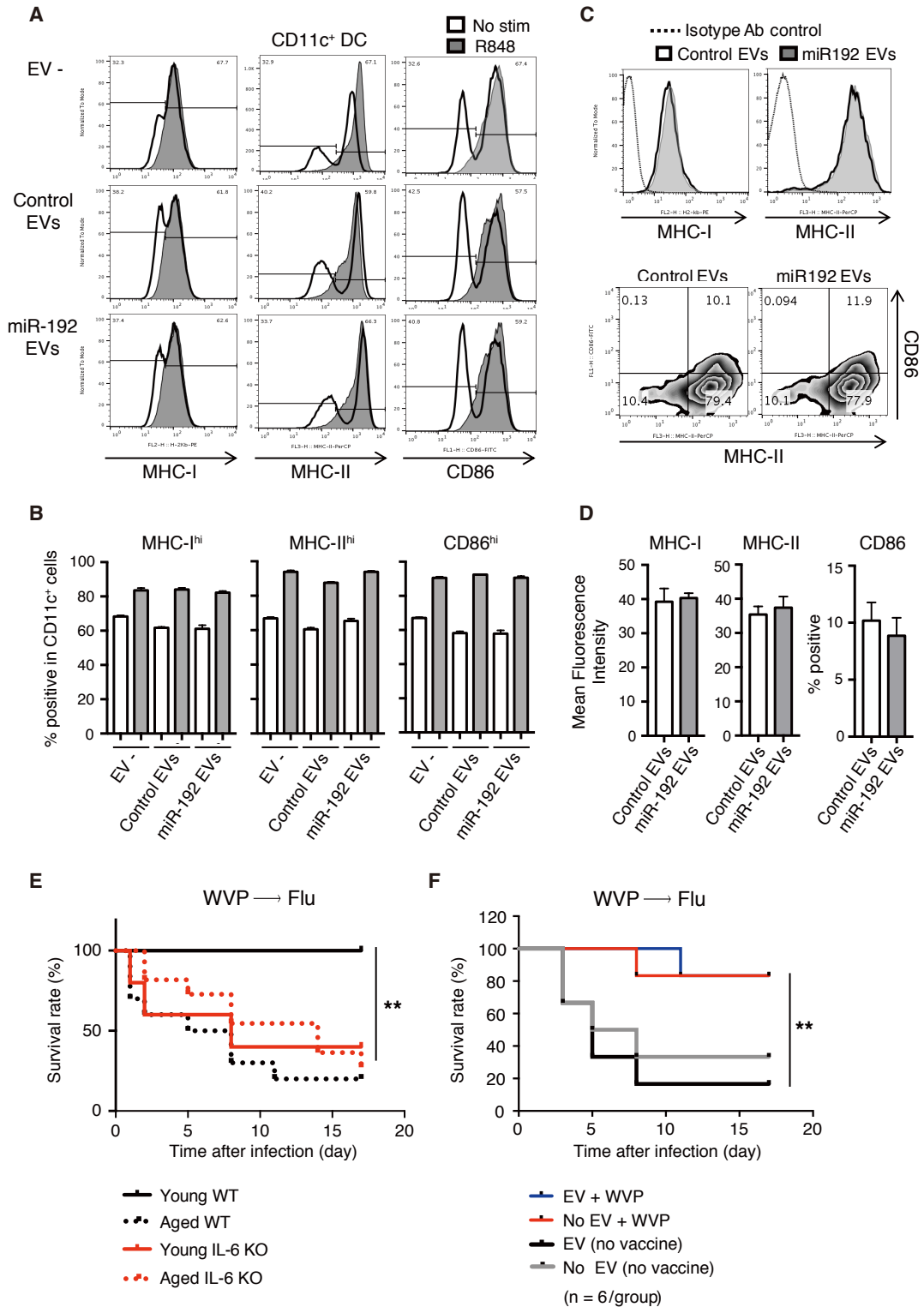

(A, B) BMDCs were treated with control EVs or miR-192-enriched EVs in vitro for 24 hr, and then were stimulated with R848. Surface expression of MHC-I, MHC-II, and CD86 were analyzed.

Representative histograms of their expression (A) and the frequencies of positive populations in $CD11c^+$ dendritic cells (B) are shown (n = 3). (C, D) Aged mice were injected with control or miR192-enriched EVs, and were inoculated with WVP. $CD11c^+$ dendritic cells were analyzed for the expression of MHC-I, MHC-II, and CD86. Representative histograms (upper panels), dot plots (lower panels) (C), and their MFIs or frequencies (D) are shown (n = 3). (E) WT and IL-6 KO young and aged mice were inoculated with WVP, and then control or miR-192 EVs were transferred into those mice. Mice were then challenged with influenza A virus (PR8), and survivals of mice were monitored (n = 6 in each group). (F) Young mice were inoculated with WVP twice with a week interval. Control mimic miRNA EVs were transferred into those mice 18 hr before WVP inoculation. Mice were challenged with lethal dose of influenza A virus (PR8), and their survival were monitored (**$p < 0.01$; n = 6 in each group). Data represent means ± SEM.

Figure S7. Th1/Th2 response after WVP inoculation, Related to Figure 8.

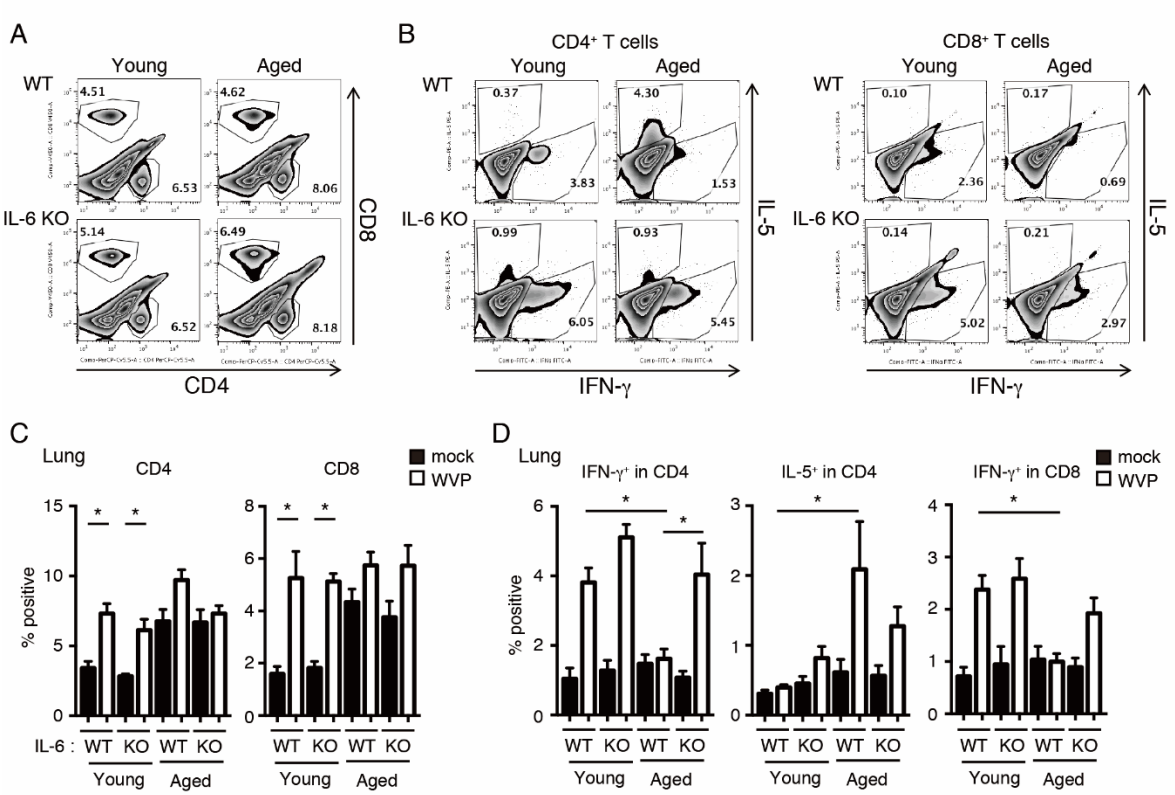

(A–D) Young and aged WT and IL-6 KO mice were inoculated with WVP. Five days later, lung tissues were analyzed for infiltrating CD4 and CD8 T cells (representative plot; A and frequencies: C), and their production of IFN-γ and IL-5 (representative dot plot: B and frequencies: D) (*$p < 0.05$; n = 5). Data represent means ± SEM.

Supplemental Table 1

The sequence of primers for quantitative real-time PCR in this study		
Gene name	Primer sequence forward (5'-3')	reverse
miR19b	**TGTGCAAATCCATGCAAAACTGA**	mRQ 3' primer from Mir-X miRNA First-Strand Synthesis kit (Clontech)
miR21	**TAGCTTATCAGACTGATGTTGA**	mRQ 3' primer
miR181c-5p	**AACATTCAACCTGTCGGTGAGT**	mRQ 3' primer
miR192-5p	**CTGACCTATGAATTGACAGCC**	mRQ 3' primer
miR322-5p	**CAGCAGCAATTCATGTTTTGGA**	mRQ 3' primer
Mouse *Gapdh*	**AATGGTGAAGGTCGGTGTG**	**GAAGATGGTGATGGGCTTCC**
Mouse *Ccl2*	**CAGCAAGATGATCCCAATGAGTAG**	**CTCCTTGAGTTGGTGACAAAAAC**
Mouse *Il6*	**TAGTCCTTCCTACCCCAATTTCC**	**TTGGTCCTTAGCCACTCCTTC**
Mouse *Tnfa*	**CATCTTCTCAAAATTCGAGTGACAA**	**TGGGAGTAGACAAGGTACAACCC**
Mouse *Il1b*	**CCGTGGACCTTCCAGGATGA**	**GGGAACGTCACACACCAGCA**
Mouse *Ifna*	**TACTCAGCAGACCTTGAACC**	**GGTACACAGTGATCCTGTGG**
Mouse *Il12b*	**AGTGTGAAGCACCAAATTACTCC**	**CCCGAGAGTCAGGGGAACT**
Human *Il6*	**AGGCACTGGCAGAAAACAAC**	**TTTTCACCAGGCAAGTCTCC**
Human *Tnfa*	**TCTTCTCGAACCCCGAGTGA**	**AGCTGCCCCTCAGCTTGA**

Transparent Methods

KEY RESOURCES TABLE

REAGENT or RESOURCE	SOURCE	IDENTIFIER
Antibodies		
I-κB (44D4) rabbit Ab	Cell Signaling Technology	Cat# 4812
Phospho-NF-κB p65(Ser536)(93H1) rabbit Ab	Cell Signaling Technology	Cat# 3033
NF-κB p65 (D14E12) rabbit Ab	Cell Signaling Technology	Cat# 8242
Phospho-IKKβ(Ser176/180)(16A6) rabbit Ab	Cell Signaling Technology	Cat# 2697
IKKβ (D30C6) rabbit Ab	Cell Signaling Technology	Cat# 8943
Phospho-p38 MAPK(Thr180/Thr182)(D3F9) rabbit Ab	Cell Signaling Technology	Cat# 8690
p38 MAPK (D3F9) rabbit Ab	Cell Signaling Technology	Cat# 4511
Phospho-p44/42 ERK1/2 (Thr202/Tyr204)(D13.14.4) rabbit Ab	Cell Signaling Technology	Cat# 4370
p42 ERK2 rabbit polyclonal Ab	Cell Signaling Technology	Cat# 9108
Phospho-TBK1(Ser172)(D52C2) Rabbit Ab	Cell Signaling Technology	Cat# 5483
TBK1 (D1B4) rabbit Ab	Cell Signaling Technology	Cat# 3504
Goat anti-mouse IgG1, HRP-conjugated	Southern Biotechnology	Cat# 1070-05
Goat anti-mouse IgG2c, HRP-conjugated	Southern Biotechnology	Cat# 1079-05
Goat anti-mouse total IgG, HRP-conjugated	Southern Biotechnology	Cat# 1030-05
Anti-β-actin monoclonal Ab (6D1)	MBL	Car# M177-3
FITC anti-mouse CD86 Ab (RB6-8C5)	BD Biosciences	Cat# 564514
PE anti-mouse H-2Kb Ab (AF6-88.5)	BD Biosciences	Cat# 553570
PE anti-mouse/human IL-5 Ab (TRFK5)	BD Biosciences	Cat# 554395
BB515 anti-mouse Siglec F Ab (E50-2440)	BD Biosciences	Cat# 564514
FITC anti-mouse Gr-1 Ab (RB6-8C5)	TONBO	Cat# 35-5931
PE anti-mouse CD45.2 Ab (104)	TONBO	Cat# 50-0454
Brilliant Violet 421 anti- mouse F4/80 Ab (BM8)	BioLegend	Cat# 123137
APC anti-mouse CD11c (N418)	BioLegend	Cat# 117309
APC-Cy7 anti-mouse Ly6C Ab (HK1.4)	BioLegend	Cat# 128026
PerCP anti-mouse/human CD11b Ab (M1/70)	BioLegend	Cat# 101230
APC-Cy7 anti-mouse CD45 Ab (30-F11)	BioLegend	Cat# 103116

PerCP/Cy5.5 anti-mouse I-A/I-E Ab (M5/114.15.2)	BioLegend	Cat# 107625
AF488 anti-mouse IFN-γ Ab (XMG1.2)	BioLegend	Cat# 554395
APC anti-mouse CD64 Ab (REA286)	Myltenyi Biotec	Cat# 130-103-879
Anti-rabbit IgG, HRP-linked whole Ab Donkey	GE Healthcare	Cat# NA934
Anti-mouse IgG, HRP-linked whole Ab Sheep	GE Healthcare	Cat# NA931
ExoAb Antibody Kit (CD63, CD9, Hsp70 Abs)	System Biosciences	Cat# EXOAB-KIT-1
Anti-mouse IL-6 Ab (MP5-20F3)	BioXCell	Cat# BE0046
Anti-mouse IL-1β Ab (B122)	BioXCell	Cat# BE0246
Anti-mouse TNF-α Ab (XT3.11)	BioXCell	Cat# BE0058
Rat IgG (control Ab)	Sigma-Aldrich	Cat# 14131
Polyclonal rabbit anti- ZEB2 Ab	proteintech	Cat# 14026-1AP
Bacterial and Virus Strains		
Influenza A virus H1N1 strain Puerto Rico/34/8(PR8)	Oshiumi H. et al., 2010	PR8 strain
Biological Samples		
Formalin-inactivated influenza vaccine from A/California/7/2009[H1N1]	KAKETSUKEN	
Chemicals, Peptides, and Recombinant Proteins		
Recombinant mouse IL-6	Wako	Cat# 097-04431
Trypsin-EDTA solution	Wako	Cat# 1689149
Penicillin-Streptomycin	Wako	Cat# 168-23191
Dulbecco's Modified Eagle's Medium (DMEM)	Wako	Cat# 043-30085
Rowell Park Memorial Institute (RPMI)	Wako	Cat# 189-02025
Phosphate-buffered saline (PBS)	Wako	Cat# 045-29795
Proteinase K solution	Wako	Cat# 162-22751
CL097	Invivogen	Cat# tlrl-c97
R848 (Resiquimod)	Sigma-Aldrich	Cat# SML0196
Lipopolysaccharides (LPS) from Salmonella enterica serotype enteritidis	Sigma-Aldrich	Cat# L7770
DNase I from bovine pancreas	Sigma-Aldrich	Cat# 11284932001
Collagenase D from Clostridium histolyticum	Sigma-Aldrich	Cat# 11088866001

Exosome isolation reagent <from cell culture media>	Thermo Fisher Scientific	REF# 4478359
Exosome isolation reagent <from serum>	Thermo Fisher Scientific	REF# 4478360
TRIzol™ RNA Isolation Reagents	Thermo Fisher Scientific	Cat# 15596026
ELISA coating buffer powder	Thermo Fisher Scientific	Cat# 00-0044-59
Exosome Spin Columns	Thermo Fisher Scientific	Cat# 4484449
SYTO RNASelect™ Green Fluorescent Cell Stain	Molecular Probes	Cat# S32703
ProLong™ Diamond Antifade Mountant with DAPI	Invitrogen	Cat# P36966
ISOkine™ Human recombinant M-CSF	ORF GENETICS	Cat# 01-A0220
TransIT TKO transfection reagent	Mirus Bio	Cat# MIR2150
Power SYBR Green PCR Master Mix	Applied Biosystems	Cat# 4367659
OPTI-MEM	GIBCO	Cat# 31985-070
ECL™ Prime blocking agent	GE Healthcare	Cat# RPN418V
ECL™ Prime Western Blotting Detection Reagents	GE Healthcare	Cat# RPN2232
PolyI:C	GE Healthcare	Cat# 27473201
Fetal Bovine Serum	SIGMA	Cat# 172012
0.45 μm MILLEX HA syringe filter unit	MILLIPORE	Cat# SLHA033SS
Pre-stained molecular weight marker	Bio-Rad	Cat# 1610393
Nitrocellulose membrane, 0.2 μm	Bio-Rad	Cat# 1620147
Protease inhibitor cocktail	Roche	Cat# 4693116001
Recombinant mouse IL-1β	R&D systems	Cat# 401-ML-025
Recombinant murine TNF-α	PEPROTECH	Cat# 315-01A
Recombinant murine GM-CSF	PEPROTECH	Cat# 315-03
Critical Commercial Assays		
Human CD14 MicroBeads	Myltenyi Biotec	Cat# 130-050-201
Human & Mouse CD11b MicroBeads	Myltenyi Biotec	Cat# 130-049-601
Anti-Ly-6G MicroBeads UltraPure	Myltenyi Biotec	Cat# 130-120-337
Mouse CD11c MicroBeads UltraPure	Myltenyi Biotec	Cat# 130-108-338
Mouse CD19 MicroBeads	Myltenyi Biotec	Cat# 130-121-301
Mouse CD4(L3T4) MicroBeads	Myltenyi Biotec	Cat# 130-117-043
Mouse CD8(Ly-2) MicroBeads	Myltenyi Biotec	Cat# 130-117-044
Anti-Biotin MicroBeads	Myltenyi Biotec	Cat# 130-097-046

Pan Exosome Isolation Kit	Myltenyi Biotec	Cat# 130-117-039
Fixation/Permeabilization Solution Kit	BD Biosciences	Cat# 554714
Quantikine Mouse IL-6 ELISA	R&D Systems	Cat# M6000B
Quantikine Mouse TNF ELISA	R&D Systems	Cat# MTA00B
Quantikine Mouse CXCL10 ELISA	R&D Systems	Cat# MCX100
RNeasy Plus Mini Kit	QIAGEN	Cat# 74104
ReverTra Ace qPCR RT Master Mix with gDNA remover	TOYOBO	Cat# FSQ-301
Taqman mouse *Ifng* assay	Applied Biosystems	Mm01168134_m1
Taqman mouse *Ifnb* assay	Applied Biosystems	Mm00439552_s1
Taqman mouse *Il10* assay	Applied Biosystems	Mm01288386_m1
Taqman mouse *Cebpb* assay	Applied Biosystems	Mm00843434_s1
Taqman Fast Universal PCR Master Mix II, no UNG	Applied Biosystems	Cat# 4352042
*mir*Vana™ miR-192-5p Mimic	Thermo Fisher Scientific	Assay ID MC10456
*mir*Vana™ miR-19b Mimic	Thermo Fisher Scientific	Assay ID MC10629
*mir*Vana™ miR-21 Mimic	Thermo Fisher Scientific	Assay ID MC10206
*mir*Vana™ miR-181c-5p Mimic	Thermo Fisher Scientific	Assay ID MC10181
*mir*Vana™ miR-322-5p Mimic	Thermo Fisher Scientific	Assay ID MC11080
*mir*Vana™ miR Mimic, negative control	Thermo Fisher Scientific	Cat# 4464059
*mir*Vana™ miR-192-5p inhibitor	Thermo Fisher Scientific	Assay ID MH10456
*mir*Vana™ miR-101c inhibitor	Thermo Fisher Scientific	Assay ID MH20630
Silencer™ Select Pre-designed *Zeb2* siRNA	Thermo Fisher Scientific	Assay ID s76956
Silencer™ Select Negative Control siRNA	Thermo Fisher Scientific	Cat# 439843
Mir-X™ miRNA First-Strand Synthesis Kit	Clontech	Cat# 638315
e-Myco™ Mycoplasma PCR Detection Kit	Minerva Biolabs GmbH	REF# 25239
BD Vacutainer CPT™ tubes	Becton, Dickinson and Company	REF# 362753
Experimental Models: Cell Lines		
Mouse macrophage line Raw264.7	ATCC	Cat#TIB-71
MDCK	ATCC	Cat#CCL-34

Experimental Models: Organisms/Strains		
IL6R-deficient mice were obtained by mating IL6R$^{flox/flox}$ mice (from Jackson Laboratory) and CAG promoter-driven Cre transgenic mice (Araki, *Nucleic Acids Res.* 2002;30:e103).	Tsukamoto et al., 2017	
Deposited Data		
Original data	Mendeley dataset	https://data.mendeley.com/datasets/f7p64t4x9d/draft?a=5af939ff-9e66-47b2-bed6-c2d8d7f4d414

CONTACT FOR REAGENT AND RESOURCE SHARING

Further information and inquiries for reagents may be directed to, and will be fulfilled by the corresponding authors Hirotake Tsukamoto (htsukamo@kumamoto-u.ac.jp) and Hiroyuki Oshiumi (oshiumi@kumamoto-u.ac.jp).

EXPERIMENTAL MODEL AND SUBJECT DETAILS

Mice

Young (2-3 months) male C57BL/6JrSlc mice were purchased from Japan SLC, Inc. IL-6-deficient mice and IL-6 receptor α-flox/flox (IL6R$^{fl/fl}$) mice were obtained from The Jackson Laboratory. Mice with ubiquitous deficiency of IL6Rα were generated by crossing of IL6R$^{fl/fl}$ mice with the mice expressing the CAG promoter-driven Cre transgene (Tsukamoto et al., 2017). Those mice were maintained for 14-18 months to utilize as aged mice. All the mice were housed in a pressure-controlled room at the Center for Animal Resources and Development, Kumamoto University, and all the experimental procedures were approved by the Institutional Animal Committee of Kumamoto University and performed in accordance with accepted guidelines.

Cell lines, viruses, and vaccines

Murine macrophage line RAW264.7 cells were provided by ATCC. Mycoplasma testing was performed using e-Myco Mycoplasma PCR Detection kit (Minerva Biolabs GmbH). Mouse-

adapted influenza A virus (IAV) H1N1 strain Puerto Rico/34/8 (PR8) was propagated as described previously (Kouwaki et al., 2017), and viral titer was assessed using MDCK cells. Formalin-inactivated influenza whole vaccine derived from A/California/7/2009[H1N1] was kindly provided by KAKETSUKEN (Kumamoto). Human monocytes were isolated from healthy adults. Cells were cultured in RPMI-1640 (Wako), and DMEM (Wako) containing 10% FCS and 1% (v/v) penicillin/streptomycin (100 units/mL of penicillin, 100 μg/mL of streptomycine; Wako) at 37 ^{o}C and 5% CO_2.

Vaccination and virus inoculation

Under anesthesia, mice were intranasally inoculated with 18 μg (/35 μL) WVP or were infected with 1 x 10^6 PFU of IAV, which corresponded to lethal dose, following two times of vaccination with WVP once a week. The mice were monitored daily for signs of illness, weight loss, and death daily for 17 days after viral infection. In some experimental settings, mice were injected with 200 μg of control IgG Ab (Millipore), or anti-F4/80 (CI:A3-1, BioXCell) plus anti-CSF1R (AFS98, BioXCell) Ab were injected intraperitoneally 1 day before and 3 or 6 days after intranasal WVP inoculation for *in vivo* macrophage depletion. For blocking inflammatory cytokine activities in vivo, 200 μg of antibody specific to IL-6, IL-1β, and TNF-α (BioXcell) were injected twice with 2 days interval into the mice before analysis.

Macrophage differentiation, transfection, and stimulation

Mouse BMMs and human monocyte-derived macrophages were generated from bone marrow cells and $CD14^+$ monocytes, respectively, by stimulation with M-CSF (50 ng/ml; ORF GENETCS) for 4-8 days. $CD14^+$ monocytes were purified from the blood of a healthy donor using BD Vacutainer CPT blood collection tubes (Becton, Dickinson Company) and CD14 microbeads (Miltenyi Biotec). Written informed consent was obtained from the donor before analysis, and this study was conducted in accordance with the principles of the Helsinki Declaration and approved by the Institutional Review Board of Kumamoto University. One hundred pmol of miR-192-5p mimic RNA, an inhibitor of miR-192, miR-101c, or negative control miRNA mimic (all from Thermo Fisher Scientific) were transfected into BMM, RAW264.7, and monocyte-derived macrophages using the TRANsit transfection reagent (Mirus Bio) according to the manufacturer's instructions. Transfection efficacy was routinely 85–90 %. After 24-36 hours of transfection, cells were stimulated with WVP, LPS, R848 (both from Sigma-Aldrich), or CL097 (Invivogen), and poly I:C (GE Healthcare).

Isolation, analysis, labeling, and transfer of EVs

EVs were isolated from the serum with total exosome isolation reagent <from serum> (Thermo Fisher Scientific) according to the manufacturer's instructions. EVs were also isolated from the 48 hr culture supernatant of miRNA mimic-transfected RAW264.7 cells with exosome isolation reagent <from cell culture media> (Thermo Fisher Scientific). When the EVs were collected from negative control miR mimic- or miR-192 mimic-transfected cells, we used FCS-free media in our all experiments. When the EVs were isolated from EDTA-treated plasma, Pan Exosome isolation kit that capture EVs with anti-CD9, CD63, and CD81 Abs (Miltenyi Biotec) were utilized. In some experiments, 100 ng of recombinant murine IL-1β (R&D systems), 200 ng of recombinant IL-6 (Wako), or TNF-α (Peprotech) were intravenously injected into the mice, followed by the isolation of serum EVs. EV size and concentration were assessed with a NanoSight NS300 (Malvern Panalytical). Each sample was diluted 10, 000 x times and were measured five times. Data were analyzed with NTA3.2 software. Isolated EVs were passed through a 0.45 μM filter, and 0.5-1.0 x 10^{10} EV particles from isolated EVs were intravenously transferred into each mouse 1 day before intraperitoneal injection of LPS (sub-lethal dose; 3 μg/mouse) in endotoxemia model or intranasal administration of WVP. For evaluating transduction of EVs, RNA contained in EVs were labeled with SYTO RNASletct Green Fluorescent Cell Stain reagent according to the manufactures' instructions, and further purified with Exosome spin column (Thermo Fisher Scientific).

Real-time PCR

Total RNA was extracted using TRIzol reagent (Thermo Fisher Scientific) and an RNeasy Plus Mini Kit (QIGEN) and reverse-transcribed with ReverTra Ace (TOYOBO). Real-time quantitative PCR (qPCR) was performed on a ViiA7 or One-Step Real-time PCR System with Taqman Universal PCR Master Mix reagents (Applied Biosystems) and TaqMan probes or, with Power SYBR Green PCR Master Mix (Applied Biosystems) using the primers listed in Supplemental Table 1. Expression levels for each gene were normalized to *Gapdh* expression using the comparative 2[-ΔΔCT] method. Levels of miRNA expression were assessed via a reverse transcription reaction for miRNA generation was performed with a miR-X miRNA First-Strand Synthesis kit (Clontech). The miRNA levels were normalized to U6 RNA expression. Absolute quantification of miR-192 copy number and plotting of a standard curve was performed by semi-quantitative RT-qPCR analysis with a serial dilution of a known concentration of miR-192 mimic.

Based on this standard curve and absolute number of EV particles per 1 μl serum, the copy number of miR-192 contained in EVs from an adjusted volume of serum was calculated.

RNA deep sequencing and microarray analysis

RNA deep sequencing and oligo DNA microarray analysis was conducted on total RNAs extracted from pooled serum-derived EVs that were isolate from mice of each group and from pooled miRNA mimic-transfected BMMs, respectively, with a RNeasy mini kit (Qiagen). Small RNA library was prepared with TruSeq small RNA Library Prep kit, according to manufactures' instruction. Briefly, size selection is performed to extract the miRNA fragments form the total RNA. The total RNA is run on an agarose gel and the band corresponding to the size of miRNAs is cut out for further processing to exclude all bigger fragments, including all mRNAs and rRNAs from the samples. The sequencing adapters are ligated to the size selected RNA molecules. miRNA fragments with ligated adapters were converted to cDNA fragments. The amplified cDNA fragments is run on agarose gel again and the band containing the molecules containing to the miRNA fragments with ligated adaptors is cut out for subsequent sequencing. RNA sequencing was performed on a HiSeq2000. The data were deposited into the DDBJ database under accession number DRA009054. Microarray analysis was performed with a 3D-Gene Mouse Oligo chip 24k (Toray Industries Inc.) and hybridization with Cy5-labeled aRNA pool was performed according to the supplier's protocols (www.3d-gene.com). Hybridization signals were assessed with a 3D-Gene Scanner and processed by 3D-Gene Extraction software (Toray Industries Inc.). Detected signals for each gene were normalized by global normalization method (the median of the detected signal intensity was adjusted to 25). Differential gene expression affected by miR-192 transfection but not by IL-6 blockade were isolated, and then gene ontology analysis and pathway analysis were performed by Gene Spring GX (Agilent Technologies, Inc.). Microarray data are available under GEO accession number GSE138758. Heatmaps to show the gene expression ratios were prepared after removing the genes with low expression levels and normalizing for each medial value between samples.

ELISA

Cell culture media from the in vitro experiments, serum, peritoneal lavage fluid, or BALF from mice were analyzed for the levels of IL-6, TNF-α, IL-1β, and CXCL-10 using an ELISA assay kit (R&D Systems) according to the manufacturer's protocols. Levels of WVP-specific total IgG, IgG1, or IgG2c in the serum of vaccinated mice were assessed by adding sera to a plate coated with

WVP in coating buffer (Thermo Fisher Scientific), and specific Abs were detected using HRP-labeled anti-isotype specific Abs (Southern Biotech Inc.).

Isolation of primary immune cells and flow cytometric analysis

Specific cell populations were separated and isolated with CD11c microbeads for DCs, CD11b microbeads for myeloid cells, Ly6G microbeads for PMN/neutrophils, CD4/CD8 microbeads for T cells, and CD19 microbeads for B cells (all from Miltenyi Biotec) in accordance with the manufacturer's instructions. Purity of each cell populations following isolation procedures were routinely 80–95 %. When the lung-infiltrating cells were analyzed, APC-Cy7-labeled anti-CD45 Ab (3 μg/mouse) were intravenously injected before euthanasia to detect and exclude the contamination of blood-circulating cells. Cells from lung tissues were prepared by enzymatic digestion with 2.5 mg/mL collagenase D (Sigma-Aldrich) and 0.1 mg/mL DNase I (Sigma-Aldrich) for 30 min at 37 ºC, and were stained with the requisite Abs for flow cytometric analyses. In LPS-induced endotoxemia model, cells were collected from peritoneal lavage fluid by washing with PBS. For intracellular cytokine staining of T cells, cell suspensions were stimulated with PMA/ionomycin for 5 hr in the presence of breferdin A. Cells were then fixed, permeabilized, stained using Cytofix/Cytoperm kit (BD Biosciences). Immunofluorescent images and the data were analyzed using FACSVerse (BD Biosciences) and FlowJo software (Tree Star), respectively. ELISA kits for detecting levels of IL-6, CXCL10, IL-1β, and TNF-α in serum or in the culture were purchased from R&D Systems.

Western blot

miRNA mimic-transfected RAW264.7, isolated EVs, or BMMs were lysed with lysis buffer (1% NP-40, 150 mM NaCl, 20 mM Tris, pH 7.4, 2 mM EDTA, 10% glycerol, 0.25% sodium deoxycholate, 1 mM sodium orthovanadate, 25 mM β-glycerophosphate, 10 mM NaF, and a protease inhibitor tablet (Roche)). Cell lysates were resolved on a 12% SDS-PAGE under the reducing conditions, and Western blot was performed with antibodies specific to I-κB, phospho-NF-κB p65, NF-κB p65 (Cell Signaling Technology), or β-actin (MBL).

Confocal analysis

RAW264.7 cells were cultured onto a cover glass in a 24-well plate for 1 day, and then transfected with miRNA mimic. After 24 h, cells were stimulated with LPS for 1-3 h, and then were fixed with 4 % paraformaldehyde, permeabilized and blocked with 0.2 % TritonX-100/ 5% FBS in PBS. Cells

were stained with anti-NF-kB p65 Ab (Cell Signaling Technology) overnight. After washing with PBS, cells were stained with secondary anti-rabbit Ig Ab (Thermo Fisher Scientific). Stained cells were covered with Prolong Diamond Antiface Mountant with DAPI (Invitrogen) and observed under a FluoView FV1200 confocal microscope (Olympus).

Statistical analysis

Multiple comparisons were performed by one-way ANOVA followed by Tukey-Kramer post-hoc tests. A Kruskal-Wallis test was used as a nonparametric alternative to ANOVA. Data were also analyzed using unpaired Student's *t*-tests when comparing two experimental groups. For statistical analysis of survival, we performed Log-rank (Mantel-Cox) test and Grehan-Breslow-Wilcoxon test to compare the survival curves. These analyses were performed using the Prism 7 for Mac OS X (Ver. 7.0) software (GraphPad Software. Inc.).

Supplemental Reference

Kouwaki, T., Okamoto, M., Tsukamoto, H., Fukushima, Y., Matsumoto, M., Seya, T., Oshiumi, H ., 2017. Zyxin stabilizes RIG-I and MAVS interactions and promotes type I interferon response. Sci. Rep. 7, 11905.